ELSEVIER

J. Non-Newtonian Fluid Mech. 118 (2004) 17–31

Journal of Non-Newtonian Fluid Mechanics

www.elsevier.com/locate/jnnfm

# Monodomain response of arbitrary aspect ratio nematic polymers in general linear planar flows

M. Gregory Forest [a,*], Qi Wang [b], Ruhai Zhou [a], Eric P. Choate [a]

[a] *Department of Mathematics, University of North Carolina at Chapel Hill, Chapel Hill, NC 27599, USA*
[b] *Department of Mathematical Sciences, Florida State University, Tallahassee, FL 32306, USA*

Received 16 April 2003; received in revised form 2 February 2004

**Abstract**

Various rheological devices (plane Couette cell, four-roll mill, film tenter) impose approximately linear, planar flow, from which nematic polymers have been characterized across ranges of flow type and strength. Theoretical predictions of monodomain responses of nematic liquids are predominantly for simple shear flows, studied from disparate scale models: continuum theory of Leslie–Ericksen, mesoscopic theory of Landau, deGennes and many others, and kinetic theory of Hess, Doi and Edwards. Our goal here is to illustrate consequences of a monodomain correspondence principle of kinetic and mesoscopic theory for nematic polymers consisting of arbitrary aspect ratio spheroids. The principle states that the bulk rheology of monodisperse nematic polymers for all linear flows in the plane of shear and any concentration can be deduced directly from a model system consisting of pure shear flow and a renormalized molecular aspect ratio parameter. The observation that there is a "trade-off" between molecule shape and flow is not new (cf. [Proc. R. Soc. London, Ser. A 102 (1922) 161; Proc. R. Soc. London, Ser. A. 146 (1934) 501; Principles of Non-Newtonian Fluid Mechanics, McGraw-Hill, London, 1974; J. Rheol. 42 (5) (1998) 1095]). Our contribution is to precisely formulate the principle in terms of the solution space of kinetic or mesoscopic models coupled with the relationship between stresses: a two-parameter model generates solutions for an entire four-parameter family of experiments. The wealth of predictions, and available numerical codes, for nematic polymer response in simple shear can be brought to bear on different flow types. We then illustrate a variety of concrete applications. As a primary example, we deduce the monodomain attractors and phase transitions versus flow-type for four-roll mill flow settings of a nematic polymer. We further provide continuous families of planar flow types of different aspect ratio liquids that have identical monodomain dynamics. Finally, we analyze pure planar extension and straining flows as a limit of the correspondence principle.


*Keywords:* Linear planar flow; Monodomain response; Nematic polymer

## 1. Introduction

Planar flow devices serve as the prototype for laminar processing conditions of nematic polymer films. Furthermore, the shear problem for nematic polymers has been studied in great detail as the testbed for comparison of theory and experiment. Indeed, the rheological benchmark of continuum, mesoscopic, and kinetic theory for liquid crystals and nematic polymers has been their ability to match laboratory shear measurements of orientation alignment and oscillatory phases, their transitions versus molecular properties and shear rate, and features of normal stress differences and shear stresses (cf. [3,5,6]). Other flow devices, such as the four-roll mill (cf. [7,8]), allow one to vary and control the relative strength of the vorticity and extensional flow components within the class of two-dimensional, approximately linear velocity fields. Our goal here is to develop precise links between the molecular orientation distribution and stresses in planar linear flows of standard devices.

The kinetic theory of Doi for spheroidal rigid macromolecules is based on the Jeffery orbit equation for the molecular axis of symmetry $\boldsymbol{m}$,

$$\dot{\boldsymbol{m}} = \hat{\boldsymbol{\Omega}} \cdot \boldsymbol{m} + a[\hat{\boldsymbol{D}} \cdot \boldsymbol{m} - \hat{\boldsymbol{D}} : \boldsymbol{mmm}], \tag{1}$$

where the geometry parameter,

$$a = \frac{r^2 - 1}{r^2 + 1}, \tag{2}$$

* Corresponding author. Tel.: +1-919-962-9606; fax: +1-919-962-9606.
*E-mail address:* forest@amath.unc.edu (M.G. Forest).

0377-0257/$ – see front matter © 2004 Elsevier B.V. All rights reserved.
doi:10.1016/j.jnnfm.2004.02.004

parametrizes the effect of the molecular aspect ratio $r = L/d$ of the length $L$ of the symmetry axis to the diameter $d$ of the circular transverse cross-section ($0 < r < 1$ and $-1 < a < 0$ for platelets, $r > 1$ and $0 < a < 1$ for rods). $\hat{\boldsymbol{\Omega}}$ is the vorticity tensor, and $\hat{\boldsymbol{D}}$ the rate-of-strain or deformation gradient of the flow. As $a$ and $\hat{\boldsymbol{D}}$ only appear through their product $a\hat{\boldsymbol{D}}$, the orientational probability distribution function (PDF) $f(\boldsymbol{m}, t)$ of the Doi kinetic theory, and all second-moment tensor models derived from Doi theory, admit a symmetry [9,10] where the molecule shape parameter $a$ and flow straining component $\hat{\boldsymbol{D}}$ can be adjusted in unison, with an identical orientational response! This observation dates back to Jeffery [1] and has been noted by many authors (c.f. [3,4,11–13]).

In this paper, we extend this observation to a more general correspondence principle: the monodomain response of all aspect ratio nematic polymers in two-dimensional linear flows (except pure extension) can be deduced from the flow-phase diagram of simple shear flow with an extended aspect ratio parameter, $\bar{a} = \omega a$, where $\omega$ is prescribed by the linear planar flow parameters (Eq. (26) below); non-vortical planar flows require a limit, discussed in Section 4.3. We remark that this correspondence principle is related to the concept of a "sliding parameter" of [14,15] in their network models of entangled polymer dynamics.

## 2. Kinetic theory

We briefly recall the Doi kinetic theory (cf. [5,10,16]) for homogeneous liquid crystal polymers (LCPs), as well as the pre-closure form of mesoscopic models derived from kinetic theory. The PDF $f(\boldsymbol{m}, t)$ denotes the probability density that the spheroidal molecule has axis of symmetry in direction $\boldsymbol{m}$ ($\|\boldsymbol{m}\| = 1$) at time $t$. We choose to measure time in units of the bulk rotational relaxation timescale,

$$t_0 = \hat{D}_r^{-1}, \tag{3}$$

which defines a *dimensionless time t utilized in the remainder of this paper*. (We note that $\hat{D}_\mathrm{r}$ has a scaling behavior with respect to aspect ratio, cf. [6], which is implicitly accounted for in the results of this paper.)

The Smoluchowski equation for $f(\boldsymbol{m}, t)$ is given by [5]:

$$\frac{Df}{Dt} = \mathcal{R}\cdot\left[D_\mathrm{r}(\boldsymbol{m})\left(\mathcal{R}f + \frac{1}{kT}f\mathcal{R}V\right)\right] - \mathcal{R}\cdot[\boldsymbol{m}\times\dot{\boldsymbol{m}}f],$$
$$\dot{\boldsymbol{m}} = \boldsymbol{\Omega}\cdot\boldsymbol{m} + a[\boldsymbol{D}\cdot\boldsymbol{m} - \boldsymbol{D}:\boldsymbol{mmm}], \tag{4}$$

where the dimensionless rotational diffusion coefficient $D_\mathrm{r}(\boldsymbol{m})$ is

$$D_\mathrm{r}(\boldsymbol{m}) = \begin{cases} 1, & \text{for constant rotary diffusivity} \\ \left(\displaystyle\int_{\|\boldsymbol{m}'\|=1}\|\boldsymbol{m}\times\boldsymbol{m}'\|\,f(\boldsymbol{m}', t)\,\mathrm{d}\boldsymbol{m}'\right)^{-2}, & \text{otherwise,} \end{cases} \tag{5}$$

which has been normalized by the average (bulk) rotational diffusion rate $\hat{D}_\mathrm{r}$, Eq. (3); $\mathcal{R} = \boldsymbol{m}\times(\partial/\partial\boldsymbol{m})$ is the rotational gradient operator; $D/Dt(\cdot)$ denotes the dimensionless material derivative $\partial/\partial t(\cdot) + \boldsymbol{v}\cdot\nabla(\cdot)$; $\boldsymbol{v} = (\boldsymbol{\Omega} + \boldsymbol{D})\boldsymbol{x}$ is a linear velocity field already scaled with respect to the rotational diffusion timescale $t_0 = \hat{D}_\mathrm{r}^{-1}$; $\boldsymbol{D}$ and $\boldsymbol{\Omega}$ denote dimensionless rate-of-strain and vorticity tensors,

$$\boldsymbol{D} = \tfrac{1}{2}(\nabla\boldsymbol{v} + \nabla\boldsymbol{v}^\mathrm{T}), \quad \boldsymbol{\Omega} = \tfrac{1}{2}(\nabla\boldsymbol{v} - \nabla\boldsymbol{v}^\mathrm{T}); \tag{6}$$

$k$ is the Boltzmann constant; $T$ the absolute temperature; $V$ the Maier–Saupe mean-field excluded-volume potential,

$$V = -\tfrac{3}{2}NkT\boldsymbol{mm} : \langle\boldsymbol{mm}\rangle, \tag{7}$$

$$\boldsymbol{M} = \langle\boldsymbol{mm}\rangle = \int_{\|\boldsymbol{m}\|=1}\boldsymbol{mm}\,f(\boldsymbol{m}, t)\,\mathrm{d}\boldsymbol{m}; \tag{8}$$

and $N$ is a dimensionless polymer concentration, which from Eq. (7) characterizes the strength of the excluded-volume potential. Below we will explicitly define a Peclet number, $Pe$, for the ratio of flow rate to molecular relaxation rate $\hat{D}_\mathrm{r}$ after we parametrize the linear velocity field.

Mesoscopic or averaged orientational properties are derived from $f$ through the second-moment orientation tensor:

$$\boldsymbol{Q} = \langle\boldsymbol{mm}\rangle - \tfrac{1}{3}\boldsymbol{I}. \tag{9}$$

A dimensionless dynamical equation for $\boldsymbol{Q}$ is then derived by taking the second moment of the kinetic Eq. (4),

$$\frac{\partial}{\partial t}\boldsymbol{Q} - \boldsymbol{\Omega}\cdot\boldsymbol{Q} + \boldsymbol{Q}\cdot\boldsymbol{\Omega} - a[\boldsymbol{D}\cdot\boldsymbol{Q} + \boldsymbol{Q}\cdot\boldsymbol{D}]$$
$$= \frac{2}{3}a\boldsymbol{D} - 2a\boldsymbol{D} : \langle\boldsymbol{mmmm}\rangle$$
$$- \frac{1}{\Lambda}\left[\boldsymbol{Q} - N\left(\boldsymbol{Q} + \frac{\boldsymbol{I}}{3}\right)\cdot\boldsymbol{Q} + N\boldsymbol{Q} : \langle\boldsymbol{mmmm}\rangle\right], \tag{10}$$

where $\Lambda$ is the usual approximation for $D_\mathrm{r}^{-1}$,

$$\Lambda = \begin{cases} 1, & \text{for constant rotary diffusivity,} \\ \left(1 - \frac{3}{2}\boldsymbol{Q} : \boldsymbol{Q}\right)^2, & \text{otherwise.} \end{cases} \tag{11}$$

Mesoscopic models derive from (10) by positing a particular closure rule for expressing the fourth moment in terms of the second moment. The caveat we require for this paper is that the closure rule itself does not depend on $a$ or $\nabla\boldsymbol{v}$, so that $a\boldsymbol{D} : \langle\boldsymbol{mmmm}\rangle$ remains linear in $a\boldsymbol{D}$, and $\boldsymbol{Q} : \langle\boldsymbol{mmmm}\rangle$ does not depend on $\nabla\boldsymbol{v}$ or $a$. All second-moment closure models we are aware of satisfy these properties. See [9] for several examples. In this way, all mesoscopic models retain the fundamental kinetic theory symmetry between molecular aspect ratio and flow gradient [10].

## 3. A correspondence principle for planar linear flows and a generalized aspect ratio parameter

### 3.1. General planar linear flow

Consider a general linear planar flow field $\boldsymbol{v}$, confined to the $x$–$y$ plane in Cartesian coordinates $\boldsymbol{x} = (x, y, z)$:

$$\boldsymbol{v} = \begin{pmatrix} p_1 & p_2 & 0 \\ p_3 & -p_1 & 0 \\ 0 & 0 & 0 \end{pmatrix} \cdot \begin{pmatrix} x \\ y \\ z \end{pmatrix}, \tag{12}$$

where $p_1$, $p_2$ and $p_3$ are arbitrary dimensionless flow parameters (recall time has been scaled by $\hat{D}_{\mathrm{r}}^{-1}$). The corresponding dimensionless vorticity and rate-of-strain tensors are

$$\boldsymbol{\Omega} = \frac{p_2 - p_3}{2} \begin{pmatrix} 0 & 1 & 0 \\ -1 & 0 & 0 \\ 0 & 0 & 0 \end{pmatrix},$$
$$\boldsymbol{D} = \begin{pmatrix} p_1 & \frac{p_2 + p_3}{2} & 0 \\ \frac{p_2 + p_3}{2} & -p_1 & 0 \\ 0 & 0 & 0 \end{pmatrix}. \tag{13}$$

It will be convenient to work with the following basis for the gradient of linear two-dimensional flows:

$$\bar{\boldsymbol{\Omega}} = \frac{1}{2} \begin{pmatrix} 0 & 1 & 0 \\ -1 & 0 & 0 \\ 0 & 0 & 0 \end{pmatrix}, \quad \bar{\boldsymbol{D}}_{\mathrm{shear}} = \frac{1}{2} \begin{pmatrix} 0 & 1 & 0 \\ 1 & 0 & 0 \\ 0 & 0 & 0 \end{pmatrix},$$
$$\boldsymbol{D}_{\mathrm{ext}} = \frac{1}{2} \begin{pmatrix} 1 & 0 & 0 \\ 0 & -1 & 0 \\ 0 & 0 & 0 \end{pmatrix}, \tag{14}$$

which correspond to the vorticity tensor ($\bar{\boldsymbol{\Omega}}$) of all two-dimensional linear flows in the $x$–$y$ plane, the rate-of-strain tensor ($\bar{\boldsymbol{D}}_{\mathrm{shear}}$) of pure two-dimensional shear, and the deformation tensor ($\boldsymbol{D}_{\mathrm{ext}}$) for pure two-dimensional extensional flow, respectively. Then, Eq. (13) can be written as:

$$\boldsymbol{\Omega} = (p_2 - p_3)\bar{\boldsymbol{\Omega}}, \quad \boldsymbol{D} = (p_2 + p_3)\bar{\boldsymbol{D}}_{\mathrm{shear}} + 2p_1\boldsymbol{D}_{\mathrm{ext}}, \tag{15}$$

so that the two-dimensional flow (12) can be represented by:

$$\boldsymbol{v} = ((p_2 - p_3)\bar{\boldsymbol{\Omega}} + (p_2 + p_3)\bar{\boldsymbol{D}}_{\mathrm{shear}} + 2p_1\boldsymbol{D}_{\mathrm{ext}}) \cdot \boldsymbol{x}. \tag{16}$$

Finally, for all flows with non-zero vorticity, we normalize with respect to the vorticity strength $p_2 - p_3$,

$$\boldsymbol{v} = Pe \left( \bar{\boldsymbol{\Omega}} + \frac{p_2 + p_3}{p_2 - p_3}\bar{\boldsymbol{D}}_{\mathrm{shear}} + \frac{2p_1}{p_2 - p_3}\boldsymbol{D}_{\mathrm{ext}} \right) \cdot \boldsymbol{x}, \tag{17}$$

which specifies *the normalized flow rate* or *Peclet number*, $Pe$ (the ratio of the norm of the vorticity flow component to the molecular relaxation rate $\hat{D}_{\mathrm{r}}$):

$$Pe = p_2 - p_3, \tag{18}$$

and *the remaining flow parameters* $((p_2 + p_3)/(p_2 - p_3), (2p_1)/(p_2 - p_3))$ *specify the planar flow type*.

We now make contact with a few standard flows associated with rheological devices.

- *Horizontal plus vertical shear*. If $p_1 = 0$, the flow is a superposition of horizontal shear ($\boldsymbol{v} = (p_2 y, 0, 0)$) and vertical shear ($\boldsymbol{v} = (0, p_3 x, 0)$):

$$\boldsymbol{v} = Pe \left( \bar{\boldsymbol{\Omega}} + \frac{p_2 + p_3}{p_2 - p_3}\bar{\boldsymbol{D}}_{\mathrm{shear}} \right) \cdot \boldsymbol{x}. \tag{19}$$

  This class of mixed shear flows has been studied by [17,18]. The *flow type* (as opposed to strength) is called *strong* if $p_2 p_3 > 0$ (in the sense that the magnitude of the strain rate exceeds the vorticity), and *weak* if $p_2 p_3 \leq 0$. In [18], a flow-type parameter $\alpha$ is introduced, which in our context is proportional to $p_2/p_3$. In this paper, we call Eq. (19) the *canonical flow*, because after a rotation of coordinates $(x, y)$, any general planar linear flow can be transformed into this two-parameter family in the rotated coordinates (see below).
- *Horizontal shear*. If $p_1 = p_3 = 0$, then $Pe = p_2$:

$$\boldsymbol{v} = Pe(\bar{\boldsymbol{\Omega}} + \bar{\boldsymbol{D}}_{\mathrm{shear}}) \cdot \boldsymbol{x}. \tag{20}$$

  This is the simple shear flow analyzed throughout the literature (cf. [6]). Our definition of the Peclet number is consistent with the usual choice

$$Pe = \hat{D}_{\mathrm{r}}^{-1}\dot{\gamma}, \tag{21}$$

  where $\dot{\gamma} = (\hat{D}_{\mathrm{r}} p_2)$ is the (dimensional) shear rate.
- *Vertical shear*. Assume $p_1 = p_2 = 0$, $Pe = -p_3$,

$$\boldsymbol{v} = Pe(\bar{\boldsymbol{\Omega}} - \bar{\boldsymbol{D}}_{\mathrm{shear}}) \cdot \boldsymbol{x}. \tag{22}$$

- *Four-roll mill flows*. Setting $p_3 = -p_2$, so that $Pe = 2p_2$, we get the four-roll mill flow:

$$\boldsymbol{v} = Pe \left( \bar{\boldsymbol{\Omega}} + \frac{p_1}{p_2}\boldsymbol{D}_{\mathrm{ext}} \right) \cdot \boldsymbol{x}. \tag{23}$$

  Detailed discussions about four-roll mill models can be found in [7,8,19,20,22]. Fig. 1 shows streamlines for several different values of $\omega = |p_1|/p_2$.

  Note that if we let $p_2 \to 0$ in the four-roll mill model, then the vorticity component vanishes, and we get the extensional flow:

$$\boldsymbol{v} = 2p_1\boldsymbol{D}_{\mathrm{ext}} \cdot \boldsymbol{x}. \tag{24}$$

  which is studied in [19,20,22].
- *Pure straining (non-vortical) flow*. If $p_2 = p_3$, then again the vorticity vanishes,

$$\boldsymbol{v} = 2(p_2\bar{\boldsymbol{D}}_{\mathrm{shear}} + p_1\boldsymbol{D}_{\mathrm{ext}}) \cdot \boldsymbol{x}. \tag{25}$$

  Pure extensional and straining flows will be analyzed below (Section 4.3) in dual limits on flow parameters and the aspect ratio parameter.

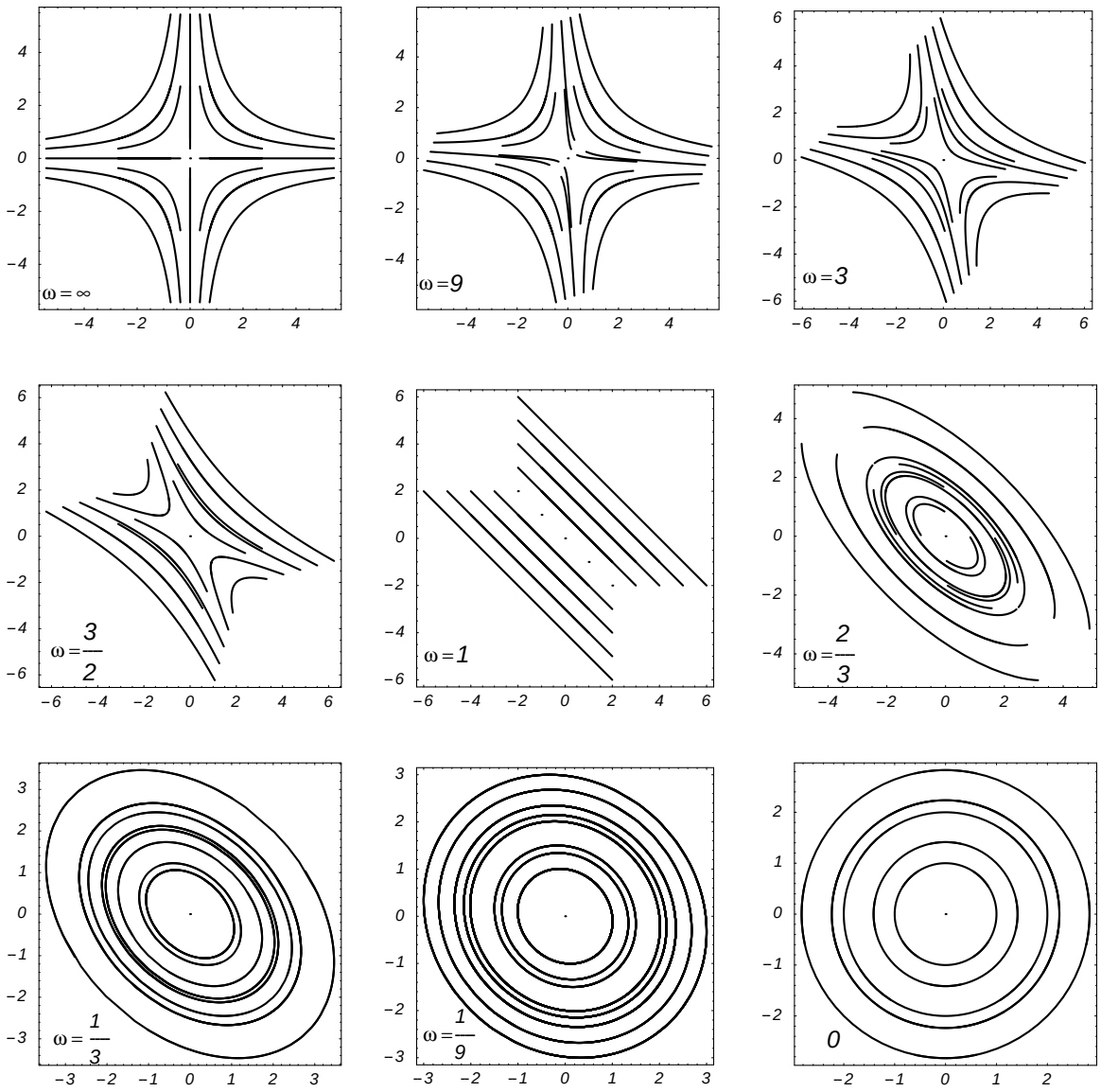


Fig. 1. Streamlines for four-roll mill flows as a function of the extension-to-vorticity parameter, $\omega = |p_1|/p_2$.

- *Planar flows with a zero deformation axis*. If $p_1^2 + p_2 p_3 = 0$, then the vorticity and rate-of-strain tensors have the same magnitude and the streamlines of the flow field are straight lines (see, e.g., the central graph in Fig. 1, where $p_1 = p_2 = -p_3$). Equivalently, $\nabla \boldsymbol{v}$ has a zero eigenvalue with multiplicity 3, and there is one axis in the $x$–$y$ plane with zero flow deformation, orthogonal to the streamlines. Pure shear is the prototype for which first ($N_1$) and second ($N_2$) normal stress differences are uniquely defined, and all of these flows with $p_1^2 + p_2 p_3 = 0$ likewise admit analogs of $N_1$ and $N_2$ (see, e.g., [3] or [21]).

### 3.2. The correspondence principle for kinetic theory

The following statement asserts the correspondence between any general planar linear flow of a nematic liquid of arbitrary aspect ratio and the horizontal shear response of nematic polymers with a renormalized aspect ratio parameter.

*If $f(\boldsymbol{m}, t)$ solves the Smoluchowski Eq. (4) with shape parameter $a$ (2) for the general planar linear flow (12), then $f(\boldsymbol{U}\boldsymbol{m}, t)$ solves the Smoluchowski equation with shape parameter*:

$$\bar{a} = \omega \cdot a, \quad \text{with}\, \omega = \frac{\sqrt{4p_1^2 + (p_2 + p_3)^2}}{p_2 - p_3}, \tag{26}$$

*for simple shear flow Eq. (20) with Peclet number Eq. (18), where $\boldsymbol{U}$ is an orthogonal matrix of rotation in the plane of flow,*

$$\boldsymbol{U} = \begin{pmatrix} \cos\delta & \sin\delta & 0 \\ -\sin\delta & \cos\delta & 0 \\ 0 & 0 & 1 \end{pmatrix}, \tag{27}$$

*with angle* $-\pi/2 < \delta \le \pi/2$ *uniquely determined by*:

$$\cos 2\delta = \frac{p_2 + p_3}{\sqrt{4p_1^2 + (p_2 + p_3)^2}},$$
$$\sin 2\delta = \frac{-2p_1}{\sqrt{4p_1^2 + (p_2 + p_3)^2}}. \tag{28}$$

We defer the proof of this statement to Appendix A.

The molecular shape parameter $a$, the flow parameters $\{p_1, p_2, p_3\}$, and the PDF $f(\boldsymbol{m}, t)$ of the Smoluchowski Eq. (4) define a *triple*:

$$(a, \{p_1, p_2, p_3\}, f(\boldsymbol{m}, t)). \tag{29}$$

If we define:

$$\bar{f}(\boldsymbol{m}, t) = f(\boldsymbol{U}\boldsymbol{m}, t), \tag{30}$$

then the above correspondence can be expressed symbolically as a mapping between *triples*:

$$(a, \{p_1, p_2, p_3\}, f(\boldsymbol{m}, t)) \to (\bar{a}, \{0, Pe, 0\}, \bar{f}(\boldsymbol{m}, t)), \tag{31}$$

assuming the vorticity is nonzero. Flows with zero vorticity require a dual limit, deferred to Section 4.3. The PDF $f(\boldsymbol{m}, t)$ for linear flow (12), parametrized by $\{p_1, p_2, p_3\}$, for molecules of aspect ratio parameter $a$, is related in a *many-to-one correspondence* with the PDF $\bar{f}$ in rotated coordinates $(\bar{x}, \bar{y}, z)^{\mathrm{T}} = U(x, y, z)^{\mathrm{T}}$, in simple shear flow $\bar{\boldsymbol{v}}(\bar{\boldsymbol{x}}) = (Pe\bar{y}, 0, 0)$, with renormalized aspect ratio $\bar{a} = \omega a$. The coordinate rotation accounts for one flow parameter, and a symmetry principle in [10] absorbs the second flow parameter. Thus, *one flow strength parameter* $Pe \neq 0$ *and one generalized aspect ratio parameter* $\bar{a}$ *suffice to determine the PDF for any planar linear flow* (*with non-zero vorticity*) *of any aspect ratio nematic liquid*.

Another way to conceptualize the parameter count goes as follows. First we rotate the $x$–$y$ plane by angle $\delta$ (clockwise if $\delta < 0$, anti-clockwise if $\delta > 0$), Eq. (28). *In the new coordinates* $\bar{x}$–$\bar{y}$, the vorticity and rate-of-strain tensors (13) become, with $\omega$ defined in (26),

$$\begin{aligned} \boldsymbol{U}\boldsymbol{\Omega}\boldsymbol{U}^{\mathrm{T}} &= \boldsymbol{\Omega} = Pe\bar{\boldsymbol{\Omega}} \\ \boldsymbol{U}\boldsymbol{D}\boldsymbol{U}^{\mathrm{T}} &= Pe\omega\bar{\boldsymbol{D}}_{\mathrm{shear}}, \end{aligned} \tag{32}$$

so that, the general linear flow Eq. (17) transforms to the canonical flow of the form: (19)

$$\bar{\boldsymbol{v}} = Pe(\bar{\boldsymbol{\Omega}} + \omega\bar{\boldsymbol{D}}_{\mathrm{shear}}) \cdot \bar{\boldsymbol{x}}. \tag{33}$$

This rotation of coordinates by angle $\delta$ leaves $\boldsymbol{\Omega}$ invariant and removes the extensional strain component $\boldsymbol{D}_{\mathrm{ext}}$, Eq. (14). If $\omega > 1$, the canonical flow-type (33) is called "strong" and "weak" if $\omega \le 1$ [17]. Simple shear is characterized by $\omega = 1$.

The second step is motivated as follows. Since the Smoluchowski equation and all corresponding mesoscopic tensor approximations have been investigated thoroughly with simple horizontal shear (20), i.e., $\omega = 1$ in (33), we seek to transform all canonical flows (33) to simple horizontal shear (20). In this way, previous results and intuition gained from shear predictions, and even existing numerical codes, can be transformed to monodomain responses in general two-dimensional linear flows. To accomplish this second step, we simply need to scale the factor $\omega$ from (33), similar to observations in [1–4], which we implement by the symmetry principle in [10]: the straining component of strength $\omega$ in (33) is mapped to 1 by scaling the aspect ratio parameter: $a \to \omega a$.

Note that the normalized shape parameter $\bar{a}$ can have any values, $\bar{a} \in \mathcal{R}$. Since $|a| < 1$ for real aspect ratios $r$, $0 < r < \infty$ (see (2)), $\bar{a}$ real with $|\bar{a}| > 1$ in a simple shear flow is equivalent to an imaginary value of $r$. Alternatively, this correspondence shows that application of the Doi theory with $|a| > 1$ in simple shear corresponds to another planar flow type of a physical aspect ratio liquid, indeed a one-parameter family of planar flows and aspect ratios linked by $\omega a =$ constant! (see below for a variety of examples). This gives credence to applications of the Doi theory for $|a| > 1$ [23] and to the use of any real shape parameter $a$, as a "sliding parameter" [7].

Fig. 2 depicts the correspondence principle graphically. Any general linear planar flow with non-zero vorticity, by (17), uniquely determines the ordered pair $((2p_1)/(p_2 - p_3), (p_2 + p_3)/(p_2 - p_3))$ (which specifies the flow type) and the Peclet number $Pe$ (which can be considered as a third coordinate transverse to the plane of Fig. 2, parametrizing strength of that flow-type). The horizontal axis represents all four-roll mill flows (23), and the vertical axis represents all canonical flows (19). Simple shear (with rate parameter $Pe = p_2$) (20) is the single point $(0, 1)$. Retaining the parameter $Pe$ transverse to Fig. 2, we

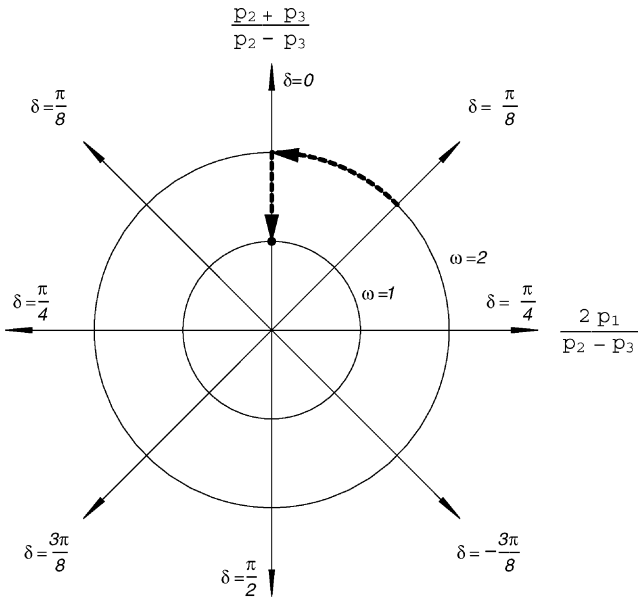


Fig. 2. Graphical illustration of the projection of the four-parameter general linear planar flow-liquid system $(p_1, p_2, p_3, a)$ onto the corresponding two-parameter simple shear flow-"liquid" system $(Pe, \bar{a})$.

want to map this entire plane onto $(0, 1)$, retaining the correspondence between kinetic theory "triples" in the process. Each point in this 2D space has "polar coordinates" determined by the rotation angle $\delta$ and the renormalization "radius" $\omega$. (The angle in this figure is determined assuming $Pe = p_2 - p_3 > 0$. If $Pe < 0$, signs of all angles should be reversed.) If we rotate the $x$–$y$ axes by the angle $\delta$, every planar flow (17) becomes a canonical flow (33) in the rotated coordinates so that the plane in Fig. 2 is mapped onto the vertical axis. Flows with zero vorticity lie at $\infty$ in Fig. 2 and are handled separately in Section 4.3. After we renormalize the aspect ratio, the canonical flow then becomes the simple shear flow, i.e., the vertical axis is then mapped onto the simple point $(0, 1)$. Since $Pe$ was arbitrary in this two-step correspondence, one retains a flow-strength degree of freedom and a renormalized aspect ratio parameter $a$.

We make a note here about the moments of the PDF. Since after the rotation step, $\boldsymbol{m}$ in the original coordinates becomes $\bar{\boldsymbol{m}} = \boldsymbol{U} \cdot \boldsymbol{m}$, we have:

$$\int_{\|\bar{\boldsymbol{m}}=1\|} \bar{\boldsymbol{m}}\bar{\boldsymbol{m}}\, f(\bar{\boldsymbol{m}})\, \mathrm{d}\bar{\boldsymbol{m}} = \boldsymbol{U}\left(\int_{\|\boldsymbol{m}=1\|} \boldsymbol{m}\boldsymbol{m}\, f(\boldsymbol{m})\, \mathrm{d}\boldsymbol{m}\right)\boldsymbol{U}^{\mathrm{T}}, \tag{34}$$

that is,

$$\bar{\boldsymbol{Q}} = \boldsymbol{U} \cdot \boldsymbol{Q} \cdot \boldsymbol{U}^{\mathrm{T}}. \tag{35}$$

For higher moments, we can establish corresponding relationships, which are particularly important for identifying mesoscopic properties of kinetic theory (Section 3.4 below).

### 3.3. The correspondence principle for mesoscopic theory

The results above clearly extend to the pre-closure averaged system (10) for any closure rule on $\boldsymbol{D} : \langle \boldsymbol{mmmm} \rangle$ and $\boldsymbol{Q} : \langle \boldsymbol{mmmm} \rangle$ that does not depend on $a$ or $\boldsymbol{v}$. To better understand the correspondence between general linear planar flow and the simple shear flow, we illustrate the results for the mesoscopic model (10) with the Doi closure:

$$\begin{aligned}\frac{\partial}{\partial t}\boldsymbol{Q} - [\boldsymbol{\Omega}\cdot\boldsymbol{Q} - \boldsymbol{Q}\cdot\boldsymbol{\Omega}] - a[\boldsymbol{D}\cdot\boldsymbol{Q} + \boldsymbol{Q}\cdot\boldsymbol{D}] &= \frac{2}{3}a\boldsymbol{D} - 2a\boldsymbol{D} : \boldsymbol{Q}\left(\boldsymbol{Q} + \frac{1}{3}\boldsymbol{I}\right) \\ &\quad - \frac{1}{\Lambda}\left[\boldsymbol{Q} - N\left(\boldsymbol{Q} + \frac{1}{3}\boldsymbol{I}\right)\cdot\boldsymbol{Q} + N\,\boldsymbol{Q} : QQ + \frac{1}{3}\boldsymbol{I}\right],\end{aligned} \tag{36}$$

where $\boldsymbol{\Omega}$ and $\boldsymbol{D}$ are given in (13), or equivalently, with $Pe = p_2 - p_3$,

$$\boldsymbol{D} = Pe\left(\frac{p_2 + p_3}{p_2 - p_3}\bar{\boldsymbol{D}}_{\mathrm{shear}} + \frac{2p_1}{p_2 - p_3}\boldsymbol{D}_{\mathrm{ext}}\right), \tag{37}$$

$$\boldsymbol{\Omega} = Pe\bar{\boldsymbol{\Omega}}. \tag{38}$$

Pre- and post-multiply the Eq. (36) by $\boldsymbol{U}$ and $\boldsymbol{U}^{\mathrm{T}}$, Eqs. (27) and (28), respectively, and notice that

$$\boldsymbol{U}\boldsymbol{Q}\boldsymbol{U}^{\mathrm{T}} = \bar{\boldsymbol{Q}}, \tag{39}$$

$$\Lambda(\boldsymbol{Q}) = \Lambda(\bar{\boldsymbol{Q}}), \tag{40}$$

$$\boldsymbol{U}(\boldsymbol{\Omega}\cdot\boldsymbol{Q} - \boldsymbol{Q}\cdot\boldsymbol{\Omega})\boldsymbol{U}^{\mathrm{T}} = (p_2 - p_3)(\bar{\boldsymbol{\Omega}}\cdot\bar{\boldsymbol{Q}} - \bar{\boldsymbol{Q}}\cdot\bar{\boldsymbol{\Omega}}), \tag{41}$$

$$\begin{aligned}&\boldsymbol{U}(\boldsymbol{D}\cdot\boldsymbol{Q} + \boldsymbol{Q}\cdot\boldsymbol{D})\boldsymbol{U}^{\mathrm{T}} \\ &\quad = \sqrt{4p_1^2 + (p_2 + p_3)^2}(\bar{\boldsymbol{D}}_{\mathrm{shear}}\cdot\bar{\boldsymbol{Q}} + \bar{\boldsymbol{Q}}\cdot\bar{\boldsymbol{D}}_{\mathrm{shear}}),\end{aligned} \tag{42}$$

$$\boldsymbol{U}\boldsymbol{D}\boldsymbol{U}^{\mathrm{T}} = \sqrt{4p_1^2 + (p_2 + p_3)^2}\,\bar{\boldsymbol{D}}_{\mathrm{shear}}, \tag{43}$$

$$\boldsymbol{U}\boldsymbol{D} : \boldsymbol{Q}\boldsymbol{Q}\boldsymbol{U}^{\mathrm{T}} = \sqrt{4p_1^2 + (p_2 + p_3)^2}\,\bar{\boldsymbol{D}}_{\mathrm{shear}} : \bar{\boldsymbol{Q}}\,\bar{\boldsymbol{Q}}, \tag{44}$$

$$\boldsymbol{U}\boldsymbol{Q}\cdot\boldsymbol{Q}\boldsymbol{U}^{\mathrm{T}} = \bar{\boldsymbol{Q}}\cdot\bar{\boldsymbol{Q}}, \tag{45}$$

$$\boldsymbol{U}\boldsymbol{Q} : \boldsymbol{Q}\boldsymbol{Q}\boldsymbol{U}^{\mathrm{T}} = \bar{\boldsymbol{Q}} : \bar{\boldsymbol{Q}}\,\bar{\boldsymbol{Q}}. \tag{46}$$

Then $\bar{\boldsymbol{Q}}$ satisfies

$$\begin{aligned}&\frac{\partial}{\partial t}\bar{\boldsymbol{Q}} - Pe[\bar{\boldsymbol{\Omega}}\cdot\bar{\boldsymbol{Q}} - \bar{\boldsymbol{Q}}\cdot\bar{\boldsymbol{\Omega}}] - \bar{a}Pe[\bar{\boldsymbol{D}}_{\mathrm{shear}}\cdot\bar{\boldsymbol{Q}} + \bar{\boldsymbol{Q}}\cdot\bar{\boldsymbol{D}}_{\mathrm{shear}}] \\ &\quad = \frac{2}{3}\bar{a}Pe\bar{\boldsymbol{D}}_{\mathrm{shear}} - 2\bar{a}Pe\bar{\boldsymbol{D}}_{\mathrm{shear}} : \bar{\boldsymbol{Q}}\left(\bar{\boldsymbol{Q}} + \frac{1}{3}\boldsymbol{I}\right) \\ &\qquad - \frac{1}{\Lambda}\left[\bar{\boldsymbol{Q}} - N\left(\bar{\boldsymbol{Q}} + \frac{1}{3}\boldsymbol{I}\right)\cdot\bar{\boldsymbol{Q}} + N\,\bar{\boldsymbol{Q}} : \bar{\boldsymbol{Q}}\,\bar{\boldsymbol{Q}} + \frac{1}{3}\boldsymbol{I}\right],\end{aligned} \tag{47}$$

which is exactly the Doi closure model in simple shear flow with shape parameter $\bar{a}$. This proof is valid for any closure rule with the caveat noted above:

*If $\boldsymbol{Q}$ is any solution to a closure form of the mesoscopic Eq. (10) with shape parameter $a$ for the general planar linear flow (12), then $\bar{\boldsymbol{Q}} \equiv \boldsymbol{U}\cdot\boldsymbol{Q}\cdot\boldsymbol{U}^{\mathrm{T}}$ is a solution to the same closure model form of (10) with shape parameter $\bar{a} = \omega a$ for simple horizontal shear.*

If we define the mesoscopic triple as in (29):

$$(a, \{p_1, p_2, p_3\}, \boldsymbol{Q}), \tag{48}$$

then the above correspondence principle can be stated symbolically as the map

$$(a, \{p_1, p_2, p_3\}, \boldsymbol{Q}) \to (\bar{a}, \{0, Pe, 0\}, \bar{\boldsymbol{Q}}). \tag{49}$$

### 3.4. The correspondence for mesoscopic properties: birefringence, major director, and stresses

Note that the order parameters of $\boldsymbol{Q}$ for the triple $(a, \{p_1, p_2, p_3\}, \boldsymbol{Q})$ are exactly the same as those of $\bar{\boldsymbol{Q}}$ for the triple $(\bar{a}, \{0, Pe, 0\}, \bar{\boldsymbol{Q}})$, since the eigenvalues of $\mathbf{Q}$ are invariant under orthogonal similarity transformations. Here, we refer *either* to $\boldsymbol{Q}(f)$ and $\bar{\boldsymbol{Q}}(\bar{f})$ extracted from the kinetic theory correspondence *or* to $\boldsymbol{Q}$ and $\bar{\boldsymbol{Q}}$ as the primitive variables of any mesoscopic closure model. This means all *birefringence and biaxiality properties* are identical in the mappings (31) and (49).

The respective frames of directors are related by the coordinate rotation,

$$\boldsymbol{n}_i = \boldsymbol{U}^{\mathrm{T}}\bar{\boldsymbol{n}}_i, \quad i = 1, 2, 3, \tag{50}$$

where $\boldsymbol{n}_i$ are directors for the triple $(a, \{p_1, p_2, p_3\}, f$ or $\boldsymbol{Q})$, and $\bar{\boldsymbol{n}}_i$ the directors for the triple $(\bar{a}, \{0, Pe, 0\}, \bar{f}$ or $\bar{\boldsymbol{Q}})$. As a consequence, *for all steady in-plane flow-aligned solutions*, the Leslie alignment angle $\phi_{\mathrm{L}}$ for $(p_1, p_2, p_3, a)$ is determined by:

$$\phi_{\mathrm{L}} = \bar{\phi}_{\mathrm{L}} + \delta, \tag{51}$$

where $\bar{\phi}_{\mathrm{L}}$ is the Leslie alignment angle for the simple shear with the triple $(\bar{a}, \{0, Pe, 0\}, \bar{\boldsymbol{Q}})$, and $\delta$ is defined in (28). We emphasize that each radial line of flow types in Fig. 2 defined by $\delta =$ constant, Eq. (28), share exactly the same Leslie flow-alignment angle $\phi_{\mathrm{L}}$ for in-plane steady states, if they exist. Whether flow-aligning (**FA**) steady states exist, and if they are stable, can be deduced from the simple shear problem with generalized aspect ratio $\bar{a}$. This analysis is discussed in detail for various mesoscopic closure models in [9,24] and for the particular Doi closure in complete generality in [25]. These existence and stability features of **FA** states vary with both $Pe$ and $\bar{a}$. We shall give explicit illustrations in the application section, including characterization of the **FA**-unsteady transitions. Analogous and more general *time dependent* monodomain responses also exist, e.g., $\phi_{\mathrm{L}}(t) = \bar{\phi}_{\mathrm{L}}(t) + \delta$ for confined in-plane solutions $f$ or $\boldsymbol{Q}$. Indeed, as we shall illustrate, *entire solution spaces* of kinetic and mesoscopic theory have precise correspondences analogous to (51).

We treat the LCP system as incompressible so that the stress tensor consists of three parts: the pressure $-p\boldsymbol{I}$, the viscous stress $\tau^{\mathrm{v}}$, and the elastic stress $\tau^{\mathrm{e}}$. The extra stress corresponding to the triple $(a, \{p_1, p_2, p_3\}, f(\boldsymbol{m}, t))$ is given by [5,6,26]:

$$\tau_{(a,\{p_1,p_2,p_3\},f(\boldsymbol{m},t))} = \tau^{\mathrm{e}}_{(a,\{p_1,p_2,p_3\},f(\boldsymbol{m},t))} + \tau^{\mathrm{v}}_{(a,\{p_1,p_2,p_3\},f(\boldsymbol{m},t))} \tag{52}$$

with

$$\tau^{\mathrm{e}}_{(a,\{p_1,p_2,p_3\},f(\boldsymbol{m},t))} = 3ackT[\boldsymbol{Q} - N(\boldsymbol{Q} + \tfrac{1}{3}\boldsymbol{I})\boldsymbol{Q} + N\boldsymbol{Q} : \langle \boldsymbol{mmmm}\rangle], \tag{53}$$

$$\tau^{\mathrm{v}}_{(a,\{p_1,p_2,p_3\},f(\boldsymbol{m},t))} = 2\eta_0\boldsymbol{D} + 3ckT[\zeta_3(a)\boldsymbol{D} + \zeta_1(a)(\boldsymbol{DM} + \boldsymbol{MD}) + \zeta_2(a)\boldsymbol{D} : \langle \boldsymbol{mmmm}\rangle], \tag{54}$$

where $\eta_0$ is the solvent viscosity,

$$\zeta_3 = \frac{\zeta^{(0)}}{I_1}, \quad \zeta_1 = \zeta^{(0)}\left(\frac{1}{I_3} - \frac{1}{I_1}\right), \quad \zeta_2 = \zeta^{(0)}\left[\frac{J_1}{I_1 J_3} + \frac{1}{I_1} - \frac{2}{I_3}\right],$$
$$r = \sqrt{\frac{1+a}{1-a}}, \quad I_1 = 2r\int_0^\infty \frac{\mathrm{d}x}{\sqrt{(r^2+x)}(1+x)^3},$$
$$I_3 = r(r^2+1)\int_0^\infty \frac{\mathrm{d}x}{\sqrt{(r^2+x)}(1+x)^2(r^2+x)},$$
$$J_1 = r\int_0^\infty \frac{x\mathrm{d}x}{\sqrt{(r^2+x)}(1+x)^3}, \quad J_3 = r\int_0^\infty \frac{x\mathrm{d}x}{\sqrt{(r^2+x)}(1+x)^2(r^2+x)}, \tag{55}$$

$\zeta^{(0)}$ is a free parameter to be experimentally characterized, and $c$ the number density of LCP molecules per unit volume. Note that the mesoscopic stresses (53) and (54) involve only the second and fourth moments of $f$, and in the case of a mesoscopic closure model, the closure rules for $\boldsymbol{Q} : \langle \boldsymbol{mmmm}\rangle$ and $\boldsymbol{D} : \langle \boldsymbol{mmmm}\rangle$ needed for (10) also uniquely specify the stress tensor.

The correspondence principle (31) or (49) gives us a mechanism to construct the extra stress tensor $\tau_{(a,\{p_1,p_2,p_3\},f(\boldsymbol{m},t))}$ or $\tau_{(a,\{p_1,p_2,p_3\},\boldsymbol{Q})}$ directly from the corresponding triple $(\bar{a}, \{0, Pe, 0\}, \bar{f}(\boldsymbol{m}, t))$ or $(\bar{a}, \{0, Pe, 0\}, \bar{\boldsymbol{Q}})$. The coordinate axes defined by the rotation matrix $\boldsymbol{U}$ given by (27) define the principle axes of deformation. In these new coordinates, the stress tensor becomes:

$$\hat{\boldsymbol{\tau}} = \boldsymbol{U}\cdot\boldsymbol{\tau}_{(a,\{p_1,p_2,p_3\},f(\boldsymbol{m},t))}\cdot\boldsymbol{U}^{\mathrm{T}} = \hat{\boldsymbol{\tau}}^{\mathrm{e}} + \omega Pe\hat{\boldsymbol{\tau}}^{\mathrm{v}}, \tag{56}$$

where

$$\left.\begin{aligned}\hat{\tau}^{\mathrm{e}} &= 3ackT[\bar{\boldsymbol{Q}} - N(\bar{\boldsymbol{Q}} + \tfrac{1}{3}\boldsymbol{I})\bar{\boldsymbol{Q}} + N\bar{\boldsymbol{Q}} : \langle \bar{\boldsymbol{m}}\bar{\boldsymbol{m}}\bar{\boldsymbol{m}}\bar{\boldsymbol{m}}\rangle],\\ \hat{\tau}^{\mathrm{v}} &= 2\eta_0\bar{\boldsymbol{D}}_{\mathrm{shear}} + 3ckT[\zeta_3(a)\bar{\boldsymbol{D}}_{\mathrm{shear}} + \zeta_1(a)(\bar{\boldsymbol{D}}_{\mathrm{shear}}\bar{\boldsymbol{M}} + \bar{\boldsymbol{M}}\bar{\boldsymbol{D}}_{\mathrm{shear}}) + \zeta_2(a)\bar{\boldsymbol{D}}_{\mathrm{shear}} : \langle \bar{\boldsymbol{m}}\bar{\boldsymbol{m}}\bar{\boldsymbol{m}}\bar{\boldsymbol{m}}\rangle].\end{aligned}\right\} \tag{57}$$

In other words, $\hat{\tau}$ in (56) is the representation of the stress tensor for the triple $(a, \{p_1, p_2, p_3\}, f(\boldsymbol{m}, t))$ in the new rotated coordinates. Note that in the above formula (57), the second and fourth moment tensors are extracted from the triple $(\bar{a}, \{0, Pe, 0\}, \bar{f}(\boldsymbol{m}, t))$, whereas the shape parameter is the real shape parameter $a$ of the LCP. In the original physical coordinates, we may rewrite (56) as:

$$\boldsymbol{\tau}_{(a,\{p_1,p_2,p_3\},f(\boldsymbol{m},t))} = \boldsymbol{U}^{\mathrm{T}}\cdot\hat{\boldsymbol{\tau}}^{\mathrm{e}}\cdot\boldsymbol{U} + \omega Pe\boldsymbol{U}^{\mathrm{T}}\cdot\hat{\boldsymbol{\tau}}^{\mathrm{v}}\cdot\boldsymbol{U}. \tag{58}$$

The apparent viscosity $\eta$, first and second normal stress differences $N_1$ and $N_2$ for the triple $(a, \{p_1, p_2, p_3\}, f(\boldsymbol{m}, t))$, are then naturally defined by the standard simple shear formulas:

$$\left.\begin{aligned}N_1 &= \hat{\tau}_{\bar{x}\bar{x}} - \hat{\tau}_{\bar{y}\bar{y}},\\ N_2 &= \hat{\tau}_{\bar{y}\bar{y}} - \hat{\tau}_{\bar{z}\bar{z}},\\ \eta &= \frac{\hat{\tau}_{\bar{x}\bar{y}}}{Pe}.\end{aligned}\right\} \tag{59}$$

This definition makes physical sense if the flow has a zero deformation axis (i.e., $p_1^2 + p_2 p_3 = 0$), in which $\bar{x}$ and $\bar{y}$ give the primary flow and flow gradient directions, respectively.

## 4. Applications

The results of Section 3 allow us to extrapolate many rheological properties *from* simple shear flow with an extended molecular aspect ratio *to* any general planar linear flow with any prescribed physical aspect ratio. They also allow one to begin with a prescribed planar flow of a given aspect ratio nematic liquid, then determine the corresponding shear rate $Pe$ and renormalized aspect ratio parameter $\bar{a}$, and solve the Smoluchowski equation in simple shear to get the response.

### 4.1. Linear flows of nematic liquids with identical monodomain attractors

The main implication of this correspondence principle is that there is a large (two continuous parameter) redundancy in monodomain responses as one considers all linear planar flows and all aspect ratio nematic liquids. As we illustrate below with several concrete examples, one can simultaneously vary flow type and molecular aspect ratio and preserve equivalent monodomain responses, with two continuous degrees of freedom. As a special case, one can fix molecular aspect ratio and vary flow type with one degree of freedom and the monodomain responses are equivalent. Furthermore, this relationship holds for all flow strengths $Pe$, Eq. (18), so that *entire flow-phase diagrams are equivalent, including all phase transitions*.

We now make this "redundancy" explicit. Suppose we solve for all triples $(\bar{a}, \{0, Pe, 0\}, \bar{f}(\boldsymbol{m}, t))$ versus nematic concentration $N$ and flow rate $Pe$, for fixed $\bar{a} \in R$. The set of all such stable solutions for fixed $\bar{a}$ comprises the simple shear phase diagram of monodomain attractors versus $(N, Pe)$, provided in [27,28] for $\bar{a} = 1$. We now want to infer a class of planar flows and physical aspect ratio liquids that share the identical phase diagram. We can therefore conclude rheological properties for a broad class of experiments without any further calculations. If the correspondence requires $\bar{a} \neq 1$, then the same numerical code can be used instead of having to derive new Galerkin expansions.

We first recall from Fig. 2 and the discussion above that any planar linear flow determined by $\{p_1, p_2, p_3\}$ for $p_2 \neq p_3$ can be parametrized by the ratio $\omega$ of rate-of-strain to vorticity and the rotation angle $\delta$. For any two parameters $\omega \geq |\bar{a}|$ (so that $|a| = |\bar{a}/\omega| \leq 1$) and $\delta \in (-\pi/2, \pi/2]$, from (18), (26) and (28), we get an explicit parametrization:

$$\begin{cases} p_1 = -\dfrac{1}{2}\omega Pe \sin 2\delta, \\ p_2 = \dfrac{1}{2}(\omega \cos 2\delta + 1)Pe, \\ p_3 = \dfrac{1}{2}(\omega \cos 2\delta - 1)Pe, \\ a = \dfrac{\bar{a}}{\omega}. \end{cases} \tag{60}$$

The correspondence principle (31) or (49) implies: for any planar flow (12), with $p_1, p_2, p_3$ given by (60), and liquids with shape parameter $a$ given by (60), *all solutions, kinetic* $(f)$ *or mesoscopic* $(\boldsymbol{Q})$, *their stability and flow-induced phase transitions, are in one-to-one correspondence with the solution* $\bar{f}$ *or* $\bar{\boldsymbol{Q}}$ *of the "liquid" with shape parameter* $\bar{a}$ *in pure shear flow with Peclet number,* $Pe$. We note $\bar{f}$ or $\bar{\boldsymbol{Q}}$ are uniquely specified by $(Pe, \bar{a})$, independent of $\delta$ and $\omega$; the values $(\delta, \omega)$ are only required to reconstruct $f$ or $\boldsymbol{Q}$ through rotation by $\boldsymbol{U}(\delta)$ and to specify the physical aspect ratio $a = \bar{a}/\omega$ of the flow (12). We now give several examples. In these examples, we will fix the concentration $N$ at a nematic value of Doi kinetic theory, $N = 6$. Other illustrations with variable $N$ are possible, but omitted.

We also note that the planar linear flow determined by (60) is hyperbolic if $\omega > 1$, elliptic if $\omega < 1$. (Fig. 1 has examples for the four-roll mill model.)

#### 4.1.1. Example 1

Suppose we fix $(Pe, \bar{a}) = (1, 2)$ in the target shear flow problem, which specifies the kinetic triple $(2, \{0, 1, 0\}, \bar{f}(\boldsymbol{m}))$. For all $(\delta, \omega) \in (-\pi/2, \pi/2] \times [2, \infty)$, we can identify by (60) a two-parameter $(\delta, \omega)$ family of kinetic theory triples,

$$(a, \{p_1, p_2, p_3\}, f(\boldsymbol{m})) = \left(\frac{2}{\omega}, \{p_1(\delta, \omega), p_2(\delta, \omega), p_3(\delta, \omega)\}, f(\boldsymbol{m})\right), \tag{61}$$

with the *identical number, type and stability of monodomain stationary distributions* $f$, or orientation tensor $\boldsymbol{Q}$ of a particular mesoscopic closure model. From kinetic simulations of the system $(2, \{0, 1, 0\}, \bar{f}(\boldsymbol{m}))$, we find that a flow-aligning PDF $\bar{f}(\boldsymbol{m})$ is the unique stable state for $N = 6$, imaged in Fig. 3 (there are also two unstable flow-aligning solutions and two unstable logrolling solutions, shown in Fig. 4 by taking a vertical slice $Pe = 1$). From $\bar{f}(\boldsymbol{m})$, we extract $\bar{\boldsymbol{Q}}(\bar{f})$ from the first three spherical harmonic amplitudes (see [10]), compute the eigenvalues and eigenvectors of $\bar{\boldsymbol{Q}}$, thereby extracting the major director $\bar{\boldsymbol{n}} = (\cos\bar{\phi}, \sin\bar{\phi}, 0)$ with $\bar{\phi}_L = 27.5^\circ$, consistent with Fig. 3.

We now vary $(\delta, \omega)$, thereby creating a surface, Fig. 5, of linear flows $(p_1, p_2, p_3)$, where attached to each planar flow $(p_1, p_2, p_3)$ on this surface is the physical aspect ratio $a = \bar{a}/\omega$ as indicated by (60). At each point on this surface, all stationary PDFs $f$ and mesoscopic tensors $\boldsymbol{Q}$ are uniquely prescribed by $\bar{f}$ or $\bar{\boldsymbol{Q}}$:

$$f(\boldsymbol{m}) = \bar{f}(\boldsymbol{U}^{\mathrm{T}} m), \quad \boldsymbol{Q} = \boldsymbol{U}^{\mathrm{T}} \cdot \bar{\boldsymbol{Q}} \cdot \boldsymbol{U}. \tag{62}$$

Note from $\boldsymbol{Q}(f)$, we immediately get $\phi_{\mathrm{L}}(\delta, \omega) = \bar{\phi}_{\mathrm{L}} + \delta$. The alignment angle is independent of $\omega$, and therefore, $\phi_{\mathrm{L}}$ is identical on the rays $\delta =$ constant in Fig. 2 or Fig. 5. *For this entire two-parameter family of flows and aspect ratio liquids, no oscillatory stationary distributions exist*, which

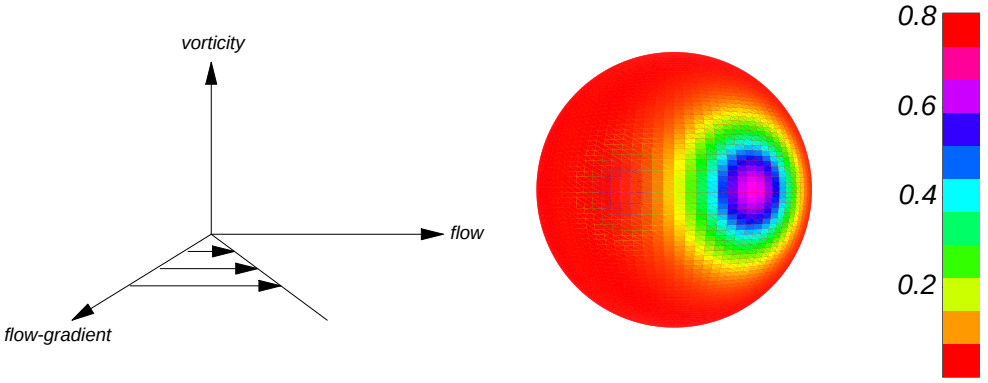


Fig. 3. The steady flow-aligned distribution function $f(\boldsymbol{m})$ for pure shear flow, $Pe = 1$, nematic concentration $N = 6$, and generalized aspect ratio $\bar{a} = 2$. This PDF is the unique stable solution for the two-parameter $(\delta, \omega)$ family of planar flows of aspect ratio liquids specified by Eq. (60). The peak orientation of the PDF defines the major director, $\boldsymbol{n}$, which lies in the (flow, flow-gradient) plane at numerically determined Leslie angle $\phi_L = 27.5^\circ$. The color bar corresponds to values of $f(\boldsymbol{m})$, $\boldsymbol{m} \in S^2$, in essence a kinetic analog of mesoscopic order parameters.

is determined solely from the solution of the single triple $(2, \{0, 1, 0\}, \bar{f}(\boldsymbol{m}))$.

Note that on this surface (Fig. 5), we have freedom to fix $\omega$, which fixes the physical aspect ratio $a$, Eq. (60), i.e., we fix the nematic liquid and the ratio of rate-of-strain to vorticity. Each fixed $\omega \geq 2$ (circles in Fig. 2) corresponds to a curve of linear flows $(p_1, p_2, p_3)(\delta)$ of a fixed nematic liquid for which the monodomain PDFs $f$ and tensors $\boldsymbol{Q}$ are identical up to rotation by $\delta$: the two green curves in Fig. 5 correspond to $\omega = 2, 2.5$, equivalently to:

$$a = 1(r = \infty) : (p_1, p_2, p_3)|_{\omega=2} = (-\sin 2\delta,\ \cos 2\delta + \tfrac{1}{2},\ \cos 2\delta - \tfrac{1}{2}), \tag{63}$$

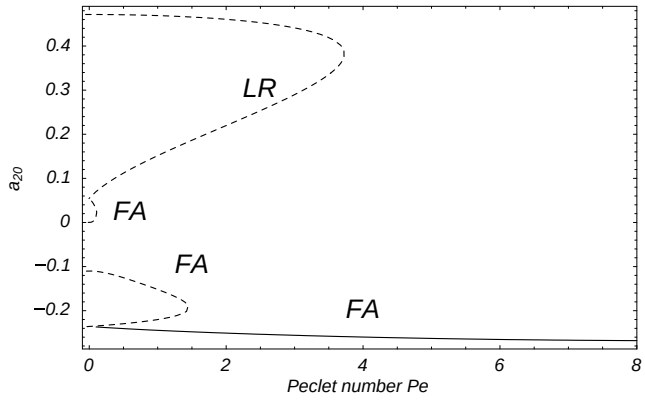


Fig. 4. The kinetic theory simple shear phase diagram for $\bar{a} = 2$, variable normalized shear rate $Pe$, nematic concentration $N = 6$, corresponding to all stationary PDFs $\bar{f}$ for $(\bar{a} = 2, \{0, Pe, 0\}, \bar{f})$. For each stationary solution $\bar{f}$, we give the value of $a_2^0$, which is proportional to $Q_{xx} + Q_{yy}$, computed by the amplitude of the PDF projection onto the spherical harmonic function $Y_2^0$. The solid line depicts the unique family of stable steady flow-aligning solutions, while dashed lines show unstable steady solutions. There are no oscillatory solutions $\bar{f}$. In the text we discuss a two-parameter family of flow types and liquids, $(a, \{p_1, p_2, p_3\}, f)$, with equivalent phase diagrams of $f$ vs. $Pe$.

and

$$a = 0.8(r = 3) : (p_1, p_2, p_3)|_{\omega=2.5} = (-\tfrac{5}{4}\sin 2\delta,\ \tfrac{1}{2}(\tfrac{5}{2}\cos 2\delta + 1),\ \tfrac{1}{2}(\tfrac{5}{2}\cos 2\delta - 1)), \tag{64}$$

Fig. 6 shows some flow streamlines for different $\delta$ with $\omega = 2$; the flow streamlines are related by a rigid rotation by $\delta$. The correspondence principle then confirms the

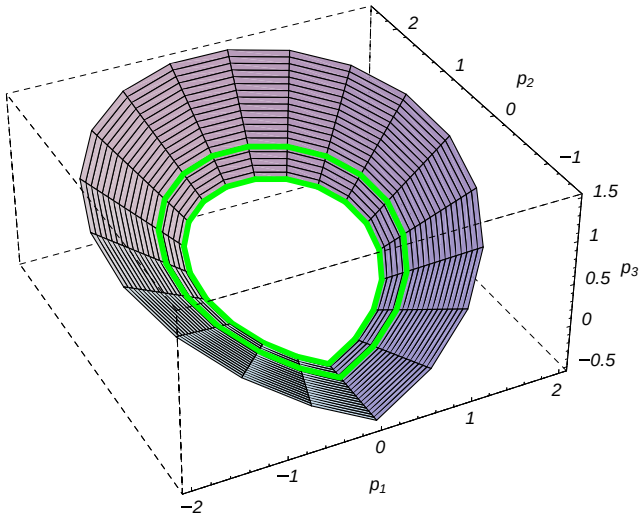


Fig. 5. A "surface" of linear flows $\boldsymbol{v}$, Eq. (17), where the flow parameters $(p_1, p_2, p_3)$ have surface coordinates $(\delta, \omega)$ according to (60). This particular surface is specified by $Pe = 1$ and $\bar{a} = 2$. Each flow prescribed by a point on this surface is associated with a specific molecular aspect ratio $(r)$ that depends only on $\omega$, $r = \sqrt{(\omega + 2)/(\omega - 2)}$. *All flows associated with this surface have equivalent monodomain dynamics*: the same number, type, and stability of stationary solutions of kinetic theory or mesoscopic closure model. Furthermore, the solutions are all given from the kinetic or mesoscopic theory with simple shear flow at fixed $Pe$ and fixed generalized aspect ratio $\bar{a}$. The two green curves inside this surface correspond to level curves $\omega = 2, 2.5$, for which more detailed properties are discussed in the text and Fig. 6.

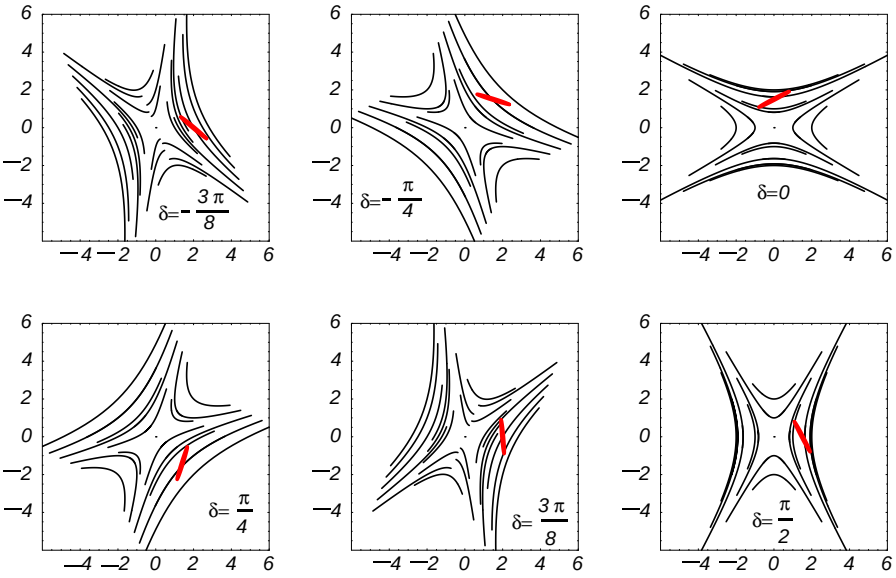


Fig. 6. Streamlines vs. flow parameter $\delta$, Eq. (28), for the linear flows defined in (60) with fixed flow strength, $Pe = 1$, and fixed ratio of rate-of-strain vs. vorticity, $\omega = 2$. These are the streamlines associated with one of the green curves ($\omega = 2$) in Fig. 5. The unique monodomain attractor when these flows are applied to infinitely thin rods at nematic concentration $N = 6$ is flow-aligning, with Leslie angle $\phi_L = 27.5^\circ + \delta$ depicted by the axis of symmetry of the red ellipses.

necessary conclusion that all of these flows induce steady flow-alignment with Leslie angle $\phi_L = \delta + \bar{\phi}_L$ with $\bar{\phi}_L = 27.5^\circ$ for $a = 1$, $N = 6$, and $Pe = 2$.

#### 4.1.2. Example 2

Rather than fix both $Pe$ and $\bar{a}$ in the target shear flow problem, we now fix only the generalized aspect ratio parameter $\bar{a} = 2$ and determine the shear-phase diagram versus $Pe$ for all triples $(2, \{0, Pe, 0\}, \bar{f})$. The numerical result is shown in Fig. 4. Once again we choose the nematic concentration $N = 6$ for this simulation (Fig. 3 depicts the unique stable flow-aligning solution at $Pe = 1$). From our correspondence principle, we now infer a two-parameter $(\delta, \omega)$ family (flow and liquid) of triples $(a, \{p_1, p_2, p_3\}, f)(\delta, \omega)$, defined by (60), *each with this identical phase diagram* versus $Pe = p_2 - p_3$. (We amplify that the only difference lies in the actual solutions associated with each branch, which are related by the constant rotation $\boldsymbol{U}(\delta)$, as defined in (27).) To give specific examples of flows and liquids with this identical phase diagram, we can fix the physical aspect ratio $a = 1$, by fixing $\omega = 2$, with $\bar{a} = 2$; another choice is $a = 0.8 (r = 3)$ with $\omega = 2.5$, and so on. Then for all $(p_1, p_2, p_3, a)$ given by (60), the solutions $f$ or $\boldsymbol{Q}$ versus $Pe = p_2 - p_3$ are equivalent to Fig. 4. As we vary flow type through $\delta \in (\pi/2, \pi/2]$, the rate-dependent phase diagram Fig. 4 is the same for the entire two-parameter family $(\delta, \omega)$.

### 4.2. Four-roll mill model

The four-roll mill invented by Taylor [2] has been explored for rheological characterization of nematic liquids in several laboratories [7,20]. Recall from Eq. (23) that this device corresponds to the restriction $p_2 + p_3 = 0$. The ratio of the rate-of-strain to vorticity is identical to our renormalization factor:

$$\omega = \frac{|p_1|}{p_2}, \tag{65}$$

and the Peclet number becomes:

$$Pe = 2p_2. \tag{66}$$

Note our parameters $(\omega, Pe)$ are related to $(\gamma, w)$ in [7] by $\omega = 1/w$, $Pe = 2\gamma/(1 + w)$, where $\gamma$ is used to measure the magnitude of the local gradient, and $w$ the ratio of vorticity to rate of strain. The streamlines of the four-roll mill for various $\omega > 0$ are shown in Fig. 1. For $\omega > 1$ the streamlines are hyperbolic. For $0 \leq \omega < 1$, the streamlines form a family of ellipses. If $\omega = 0$ ($p_1 = 0$), the flow is purely rotational; and when $\omega = \infty$ ($p_2 = 0$), the flow is purely extensional. As $\omega$ varies between 0 and $\infty$, the flow is a linear superposition of pure rotation and pure extension.

Recall the four-roll mill is represented by the horizontal axis in Fig. 2. The rotation angle $\delta$ determined by the correspondence is always $-45^\circ$ for $p_1 > 0$ or $45^\circ$ for $p_1 < 0$. The transformation matrix $\boldsymbol{U}$, Eq. (27), is then, for $p_1 > 0$,

$$\boldsymbol{U}_{\text{mill}} = \frac{\sqrt{2}}{2}\begin{pmatrix} 1 & -1 & 0 \\ 1 & 1 & 0 \\ 0 & 0 & \sqrt{2} \end{pmatrix}. \tag{67}$$

We take $\delta = \pi/4$ in formula (60), then the four-roll mill model can be parametrized by $Pe$ and $\omega$ in the following way:

$$\begin{cases} p_1 = -\dfrac{1}{2}\omega Pe, \\ p_2 = \dfrac{1}{2}Pe, \\ p_3 = -\dfrac{1}{2}Pe, \\ a = \dfrac{\bar{a}}{\omega}. \end{cases} \tag{68}$$

We now deduce various monodomain properties of four-roll mill flows of different aspect ratio nematic liquids from the target shear problem.

*4.2.1. Example 3*

Suppose we seek the entire four-roll mill monodomain phase diagram of a fixed aspect ratio liquid, e.g., $a = 1$ or 0.8, and fixed flow type ($\omega$ = constant.), allowing for variable flow rate ($Pe = 2p_2$). From (68), all kinetic triples $(a, \{p_1, p_2, p_3\}, f)$ are determined from the $Pe$-dependent shear diagram for the triple $(\bar{a}, \{0, Pe, 0\}, \bar{f})$. Fig. 7 depicts all stable (solid) and unstable (dashed) solutions for $\bar{a} = 1$, $N = 6$, and variable $Pe$. For any physical aspect ratio $a$, if we let the ratio of rate-of-strain to vorticity be chosen so that $\omega a = \bar{a} = 1$, then the four-roll mill shares this $Pe$-dependent phase diagram. For example, for discotic molecules with $a = -1, -0.8, -0.5$, or rod-like molecules with $a = 1, 0.8, 0.5$, the corresponding flow types are determined by $\omega = -1, -1.25, -2$ for discotics or $\omega = 1, 1.25, 2$ for rods, respectively; then all six of these distinct four-roll

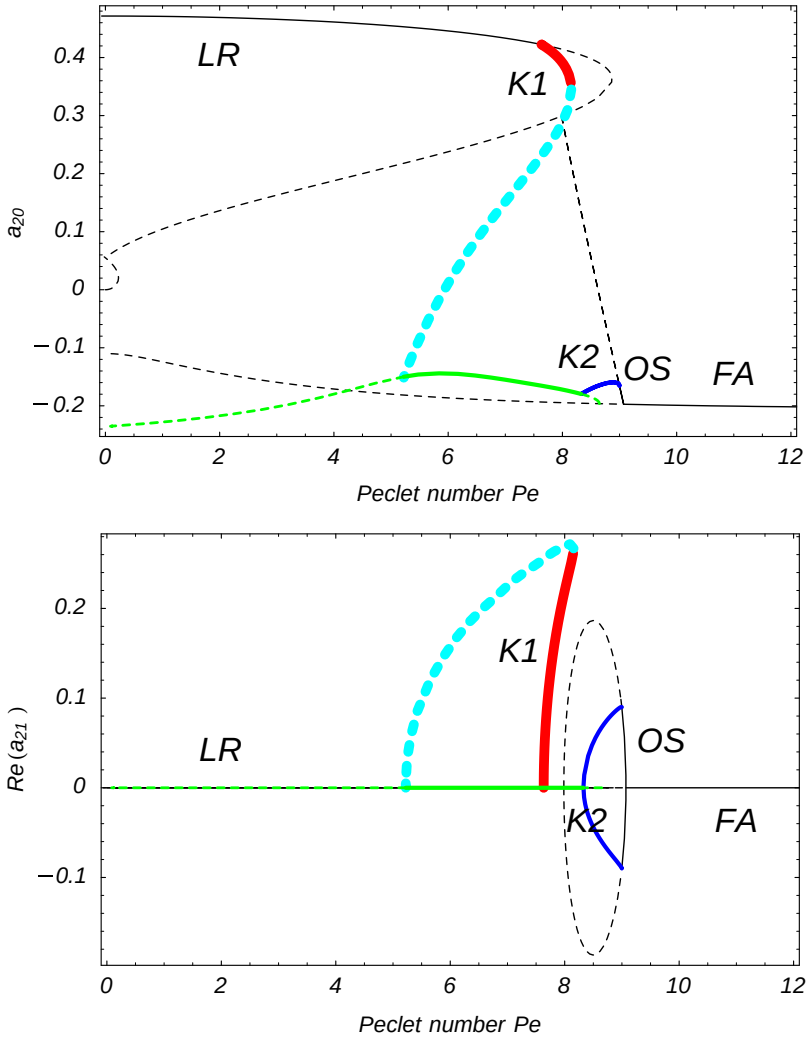


Fig. 7. The kinetic bifurcation diagram computed from kinetic theory $(\bar{a} = 1, \{0, Pe, 0\}, \bar{f})$ with nematic concentration $N = 6$ in simple shear flow of infinitely thin rods. $a_{20}$ is the projection of the PDF $\bar{f}$ onto the spherical harmonic function $Y_2^0$; $a_{21}$ the projection of $\bar{f}$ onto $Y_2^1$. These attractors (solid curves), unstable states (dashed), and phase transitions are shared by a two-parameter $(\delta, \omega)$ family, Eq. (60), of linear flows and aspect ratios, as explained in the text. Notice the dramatic difference between the attractors and phase transitions of Fig. 4, where the only difference is $\bar{a} = 2$ vs. $\bar{a} = 1$. The attractors are labeled **LR** for logrolling steady states (major director aligned with the vorticity axis), $\boldsymbol{K}_1$ for kayaking (periodic rotation of the major director around the vorticity axis), $\boldsymbol{K}_2$ for tilted kayaking, **OS** for out-of-plane steady states, **TW** for tumbling/wagging, and **FA** for in-plane steady flow-alignment. The $\boldsymbol{K}_2$ and **OS** attractors occur in *pairs*, mirror-symmetric with respect to the plane of deformation.

Table 1
Stable kinetic theory responses for variable aspect ratio parameter $\bar{a}$ with fixed concentration $N = 6$, and fixed $Pe = 8.5$

| | | | | |
|---|---|---|---|---|
| $\bar{a}$ | (0, 0.764) | (0.764, 0.932) | (0.932, 0.959) | (0.959, 0.998) |
| State(s) | **LR** | **LR/TW** | **TW/K1** | **TW** |
| $\bar{a}$ | (0.998, 1.057) | (1.057, 1.081) | (1.081, $\infty$) | |
| State(s) | **K2** | **OS** | **FA** | |

Table 2
Four-roll mill monodomain attractors and phase transitions due to flow-type variations in $\omega$, with $N = 6$, $r = \sqrt{19}$, $Pe = 8.5$

| | | | | |
|---|---|---|---|---|
| $\omega$ | (0, 0.849) | (0.849, 1.036) | (1.036, 1.066) | (1.066, 1.109) |
| State(s) | **LR** | **LR/TW** | **TW/K1** | **TW** |
| $\omega$ | (1.109, 1.174) | (1.174, 1.201) | (1.201, $\infty$) | |
| State(s) | **K2** | **OS** | **FA** | |

mill flow experiments share the *Pe*-dependent phase diagram Fig. 7.

#### 4.2.2. Example 4

As another application, we show how to *determine phase transition boundaries versus aspect ratio a* and *flow-type* $\omega$ *for four-roll mill flows from knowledge of monodomain transitions in pure shear*. Suppose, under pure shear flow, a monodomain transition happens at aspect ratio $\bar{a}$ for fixed $Pe = Pe^*$; i.e., $(\bar{a}, \{0, Pe^*, 0\}, \bar{f})$ corresponds to *a bifurcation* where attractors $\bar{f}$ undergo a transition. Then by (68), the identical transition will occur at the same $Pe^*$ if:

$$\omega a = \bar{a}, \tag{69}$$

which is a prescription for the continuation of transition curves. To illustrate, we numerically solve the kinetic PDF equation for $\bar{f}$ with $N = 6$ and $Pe = 8.5$ and search for monodomain attractor transitions due to variable shape parameter $\bar{a}$; the results are listed in Table 1. For the specific value $Pe^* = 8.5$, the solution space contains a variety of monodomain transitions at indicated values $\bar{a}$: logrolling (**LR**) to kayaking ($\boldsymbol{K}_1$), tumbling/wagging (**TW**) to tilted kayaking ($\boldsymbol{K}_2$), tilted kayaking to out-of-plane (**OS**) steady solutions, and out-of-plane to in-plane flow-aligning (**FA**) solutions. These phase transitions each persist along curves $\omega a = \bar{a} = 0.764, 0.932, 0.959, 0.998, 1.057, 1.081$, respectively, as shown in Fig. 8. For example, the **LR** to $\boldsymbol{K}_1$ transition, with bi-stable **TW**, persists for all flow-types $\omega$ and aspect ratios $a$ with $\omega a = 0.932$, at the same $Pe^* = 8.5$, with $N = 6$. The flow parameters are given by $(p_1, p_2, p_3) = (1/2)Pe(-\omega, 1, -1)$. We may further fix the molecule geometry, e.g., specify $a = 0.9$ (equivalently $r = \sqrt{19}$). Then as $\omega = \bar{a}/a$ varies in the four-roll mill model, *the flow-induced monodomain transition sequence* of Table 1 ensues, as listed in Table 2. (Alternatively, we can fix the flow type, $\omega =$ constant, and vary the molecular aspect ratio $a = \bar{a}/\omega$, and then the identical transition sequence occurs again due to variation in molecular shape.)

#### 4.2.3. Example 5

As an example of the application of the stress formula developed in the last section, we choose $\bar{a} = 0.9$, $N = 6$. Using kinetic theory, we have computed that for the simple shear model determined by the triple $(\bar{a} = 0.9, \{0, Pe, 0\}, \bar{f})$, flow-aligning states are the unique attractors when $Pe > 13.7$. Then, *for all* $\omega$, the four−roll mill model determined by the triple

$$(a, \{p_1, p_2, p_3\}, f) = \left(a = \frac{0.9}{\omega}, \left\{-\frac{1}{2}\omega Pe, \frac{1}{2}Pe, -\frac{1}{2}Pe\right\}, f\right), \tag{70}$$

has unique flow-aligning attractors when $Pe > 13.7$ with specific properties given by the correspondence principle (31). If we let $\omega = \pm 1$, i.e., $p_1 = \pm p_2$, then $p_1^2 + p_2 p_3 = 0$, for which the flow and flow gradient directions are orthogonal and fixed. From the stress tensor formula (56) and (57), the first and second normal stress differences $N_1$, $N_2$ and the apparent viscosity $\eta$ are plotted in Fig. 9 for $\omega = 1$. We conclude from these results that $N_2 < 0$ and $\eta$ increases slightly with higher flow rate. The most striking prediction is that $N_1$ changes sign, from negative to positive, at a critical *Pe* along these **FA** attractors! Thus, the often-reported sign changes in $N_1$ associated with shear-rate-dependent monodomain transitions (cf. [6]) are predicted to occur in four-roll mills *within* ***FA*** steady responses. Here we have used the correspondence to infer analogs of $N_1$ and $N_2$.

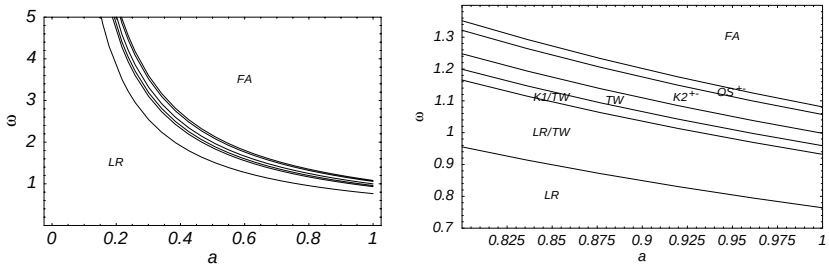


Fig. 8. All stable states for the family of four-roll mill flows with fixed flow-rate $Pe = 8.5$ and nematic concentration $N = 6$, depicted vs. extension-to-vorticity parameter $\omega$ and molecular aspect ratio parameter $a$. Seven different monodomain phase transitions occur on the curves shown. The right figure is the blow-up of the phase transition boundaries for $0.8 \leq a \leq 1$, together with the unique and bi-stable attractors in each parameter domain.

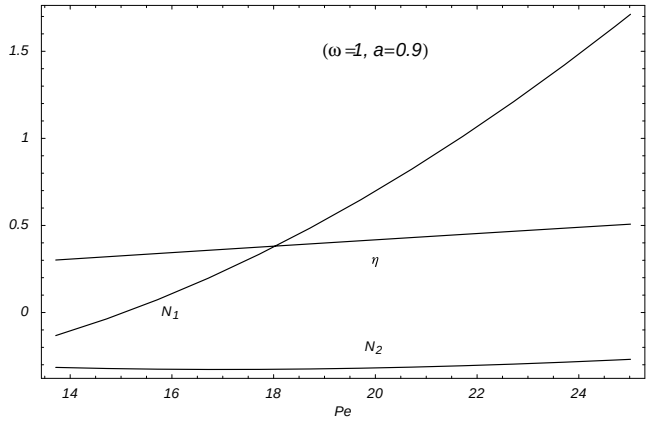


Fig. 9. Rheological predictions of four-roll mill flows in the **FA** regime with streamline geometry $\omega = 1$, where the corresponding physical aspect ratio ($r = \sqrt{(1+a)/(1-a)} = \sqrt{19}$). First and second normal stress differences, $N_1$, $N_2$, and the apparent viscosity, $\eta$, associated with stable flow-aligned monodomains of kinetic theory, with fixed nematic concentration $N = 6$, depicted vs. monodomain flow-rate $Pe$. The left endpoint of these curves corresponds to onset of flow-aligning attractors (from out-of-plane steady states), whereas the right endpoint is chosen arbitrarily since ***FA*** states persist for $Pe > 13.7$.

### 4.3. Pure straining flow

For pure straining flows ($p_2 = p_3$), (25), the correspondence principle discussed in Sections 3.2 and 3.3 needs to be refined because we have normalized with respect to the vorticity strength, $p_2 - p_3$. First we point out that any pure straining flow can be mapped to the pure extensional flow (24) by a rotation of the flow and flow-gradient plane. To see this, we simply use the rotation matrix $\boldsymbol{U}$ defined in (27) to transform all pure straining flow, $p_2 = p_3$ (including pure extensional flow, $p_2 = p_3 = 0$) to:

$$\bar{\boldsymbol{v}} = 2\sqrt{p_1^2 + p_2^2}\,\bar{\boldsymbol{D}}_{\text{shear}} \cdot \bar{\boldsymbol{x}}. \tag{71}$$

In our correspondence, relationships between $Pe, \bar{a}, \delta$ and $\{p_1, p_2, p_3\}$ can be written in the following way:

$$\bar{a}Pe = a\sqrt{4p_1^2 + (p_2 + p_3)^2}, \tag{72}$$

$$Pe = p_2 - p_3, \tag{73}$$

and $\delta$ is the rotation angle defined in (28). If we let $Pe \to 0$ in the canonical flow (33), we clearly get the pure straining flow (71), but the constraint (72) requires we simultaneous have $\bar{a} \to \infty$ with finite product $\bar{a}Pe = 2a\sqrt{p_1^2 + p_2^2}$.

To summarize, pure planar straining flows of nematic liquids with aspect ratio parameter $a$, $|a| \le 1$, correspond to a "nematic liquid" with aspect ratio parameter $\bar{a} \to \infty$ in simple shear flow with vanishing flow rate $Pe \to 0$, such that $\bar{a}Pe = 2a\sqrt{p_1^2 + p_2^2}$. The correspondence in terms of kinetic triples is:

$$(a, \{p_1, p_2, p_3\}, f) \leftrightarrow \lim_{Pe \to 0} \left( \frac{2a\sqrt{p_1^2 + p_2^2}}{Pe}, \{0, Pe, 0\}, \bar{f} \right). \tag{74}$$

To illustrate, we numerically calculate stable steady states for $a = 1$ in pure planar extensional flow with $p_1 = 100$ and $p_2 = p_3 = 0$, using the Doi closure model for $N = 6$. The solution is:

$$\boldsymbol{Q} = \begin{pmatrix} 0.664238 & 0 & 0 \\ 0 & -0.332515 & 0 \\ 0 & 0 & -0.331723 \end{pmatrix}. \tag{75}$$

Then we numerically compute the stable steady state for $\bar{a} = 10^6$, $Pe = 2 \cdot 10^{-4}$ in pure shear. The result is:

$$\bar{\boldsymbol{Q}} = \begin{pmatrix} 0.165863 & 0.498378 & 0 \\ 0.498378 & 0.165862 & 0 \\ 0 & 0 & -0.331725 \end{pmatrix}. \tag{76}$$

The rotation angle in $\boldsymbol{U}$, (27), is $\delta = -\pi/4$, which maps $\bar{\boldsymbol{Q}}$ to $\boldsymbol{Q}$.

$$\boldsymbol{Q} = \boldsymbol{U}^{\mathrm{T}} \bar{\boldsymbol{Q}} \boldsymbol{U} = \begin{pmatrix} 0.664240 & -5 \times 10^{-7} & 0 \\ -5 \times 10^{-7} & -0.332516 & 0 \\ 0 & 0 & -0.331725 \end{pmatrix}. \tag{77}$$

## 5. Conclusion

We have precisely formulated and applied a correspondence principle that relates monodomain response between shear flow and linear planar flows of spheroidal nematic fluids. The principle is valid for the Doi–Hess kinetic theory and all mesoscopic closure models derived from it. Whereas, numerous authors have noted this observation, the aim of this paper is to show both simplicity and depth in the consequences of this principle. We have illustrated how to solve the four-roll mill flow of a nematic liquid from an existing kinetic theory code for pure shear. We have shown how to search for monodomain phase transitions, e.g., flow-aligning to kayaking, which result from varying the flow type of a fixed nematic liquid. Various other applications are illustrated, including how to solve pure extensional flow by a dual limit of shear with vanishing shear rate and unphysical aspect ratio parameter. Finally, we have provided the correspondence between stress tensors in a pure shear flow and linear planar flows, which affords analogs of normal stress differences and shear stress in special cases. Table 3 schematically represents the correspondence. The first row corresponds to a general linear flow, defined in (12) and determined by three flow parameters $\{p_1, p_2, p_3\}$; $a$ is the physical LCP aspect ratio parameter; $f$ and $\boldsymbol{Q}$ are the corresponding solutions of the kinetic and mesoscopic Eqs. (4) and (10). The second row corresponds to simple shear flow

Table 3
Any linear planar flow $\{p_1, p_2, p_3\}$ of a nematic polymer with aspect ratio parameter $a$ (the first row) can be transformed to a simple shear flow with Peclet number $Pe$ defined in (18) by a rotation (27) and a renormalized aspect ratio parameter $\bar{a}$, (26)

| $p_1$ | $p_2$ | $p_3$ | $a$ | $f$ | $\boldsymbol{Q}$ |
|---|---|---|---|---|---|
| 0 | $Pe$ | 0 | $\bar{a}$ | $\bar{f}$ | $\bar{\boldsymbol{Q}}$ |

The PDFs and second-moment tensors then explicitly related by the correspondence principle of kinetic and mesoscopic theory, given in the text.

with flow rate $Pe$; $\bar{a}$ is the renormalized molecule geometry parameter (26); $\bar{f}$ and $\bar{\boldsymbol{Q}}$ are the corresponding solutions to the kinetic theory or mesoscopic tensor model in simple shear. In this correspondence, the nematic polymer concentration $N$ is fixed, but arbitrary. This fact is nontrivial since nematic polymers at rest have a rich equilibrium phase diagram versus concentration, whose fate in shear flow is quite complex (c.f., [16,27,28]). The illustrations given here show how this shear behavior maps across the space of planar linear flows, but one must keep track of the molecule aspect ratio as the flow parameters vary. The principle can be exploited in other ways, also illustrated. For example, one may posit a desired flow response mode of a given nematic polymer, such as kayaking or flow-aligning or even chaotic. From the shear flow-phase diagram, one can then prescribe families of flow-types and -rates with the prescribed monodomain response mode.

## Appendix A. A proof of the kinetic correspondence principle

We suppose $f(\boldsymbol{m}, t)$ is the solution of the Smoluchowski equation under the general planar linear flow as defined in (12). For the orthogonal matrix $\boldsymbol{U}$ given in (27), define:

$$\boldsymbol{n} = \boldsymbol{U}\boldsymbol{m}, \tag{A.1}$$

for any unit vector **m**. Also, define a new function:

$$\bar{f}(\boldsymbol{n}, t) = f(\boldsymbol{U}^{\mathrm{T}}\boldsymbol{n}, t) = f(\boldsymbol{m}, t). \tag{A.2}$$

We first notice the following chain-rule formulas for derivatives:

$$\frac{\partial}{\partial \boldsymbol{m}}\bar{f}(\boldsymbol{n}, t) = \boldsymbol{U}^{\mathrm{T}} \cdot \frac{\partial}{\partial \boldsymbol{n}}\bar{f}(\boldsymbol{n}, t), \tag{A.3}$$

$$\frac{\partial}{\partial \boldsymbol{m}} \cdot \bar{f}(\boldsymbol{n}, t) = \boldsymbol{U} \cdot \left(\frac{\partial}{\partial \boldsymbol{n}} \cdot \bar{f}(\boldsymbol{n}, t)\right). \tag{A.4}$$

Also, we write:

$$\mathcal{R}_m = \boldsymbol{m} \times \frac{\partial}{\partial \boldsymbol{m}}, \quad \mathcal{R}_n = \boldsymbol{n} \times \frac{\partial}{\partial \boldsymbol{n}}, \tag{A.5}$$

and the Maier–Saupe potential as

$$V_{\boldsymbol{m}}(f(\boldsymbol{m}, t)) = -\frac{3NkT}{2}\boldsymbol{m}\boldsymbol{m} : \int_{\|\boldsymbol{m}\|=1} \boldsymbol{m}\boldsymbol{m} f(\boldsymbol{m}, t)\, \mathrm{d}\boldsymbol{m}. \tag{A.6}$$

Notice that,

$$\begin{aligned} &V_{\boldsymbol{m}}(f(\boldsymbol{m}, t)) \\ &= -\frac{3NkT}{2}(\boldsymbol{U}\boldsymbol{m})(\boldsymbol{U}\boldsymbol{m}) : \int_{\|\boldsymbol{m}\|=1} (\boldsymbol{U}\boldsymbol{m})(\boldsymbol{U}\boldsymbol{m})\bar{f}(\boldsymbol{U}\boldsymbol{m}, t)\, \mathrm{d}\boldsymbol{m} \\ &= -\frac{3NkT}{2}\boldsymbol{n}\boldsymbol{n} : \int_{\|\boldsymbol{n}\|=1} \boldsymbol{n}\boldsymbol{n}\bar{f}(\boldsymbol{n}, t)\, \mathrm{d}\boldsymbol{n} = V_{\boldsymbol{n}}(\bar{f}(\boldsymbol{n}, t)). \end{aligned} \tag{A.7}$$

Therefore, by the chain rule,

$$\frac{\partial}{\partial \boldsymbol{m}} V_{\boldsymbol{m}}(f(\boldsymbol{m}, t)) = \frac{\partial}{\partial \boldsymbol{m}} V_{\boldsymbol{n}}(\bar{f}(\boldsymbol{n}, t)) = \boldsymbol{U}^{\mathrm{T}} \cdot \frac{\partial}{\partial \boldsymbol{n}} V_{\boldsymbol{n}}(\bar{f}(\boldsymbol{n}, t)),$$

$$\begin{aligned} &\frac{\partial}{\partial \boldsymbol{m}} \cdot \frac{\partial}{\partial \boldsymbol{m}} V_{\boldsymbol{m}}(f(\boldsymbol{m}, t)) \\ &= \frac{\partial}{\partial \boldsymbol{m}} \cdot \frac{\partial}{\partial \boldsymbol{m}} V_{\boldsymbol{n}}(\bar{f}(\boldsymbol{n}, t)) = \frac{\partial}{\partial \boldsymbol{n}} \cdot \frac{\partial}{\partial \boldsymbol{n}} V_{\boldsymbol{n}}(\bar{f}(\boldsymbol{n}, t)). \end{aligned}$$

The Smoluchowski equation can be written as:

$$\begin{aligned} &\frac{\mathrm{d}}{\mathrm{d}t} f(\boldsymbol{m}, t) \\ &= D_{\mathrm{r}}(a)\frac{\partial}{\partial \boldsymbol{m}}\left[\frac{\partial}{\partial \boldsymbol{m}} f(\boldsymbol{m}, t) + \frac{1}{kT} f(\boldsymbol{m}, t)\frac{\partial}{\partial \boldsymbol{m}} V_m(f(\boldsymbol{m}, t))\right] \\ &\quad - \frac{\partial}{\partial \boldsymbol{m}}[\dot{\boldsymbol{m}} f(\boldsymbol{m}, t)]. \end{aligned} \tag{A.8}$$

Since $f(\boldsymbol{m}, t)$ is the solution to the Smoluchowski equation with general linear flow,

$$\begin{aligned} &\frac{\mathrm{d}}{\mathrm{d}t}\bar{f}(\boldsymbol{n}, t) \\ &= \frac{\mathrm{d}}{\mathrm{d}t} f(\boldsymbol{m}, t) \\ &= D_{\mathrm{r}}(a)\frac{\partial}{\partial \boldsymbol{m}} \cdot \left[\frac{\partial}{\partial \boldsymbol{m}} f(\boldsymbol{m}, t) + \frac{1}{kT} f(\boldsymbol{m}, t)\frac{\partial}{\partial \boldsymbol{m}} V_m(f(\boldsymbol{m}, t))\right] \\ &\quad - \frac{\partial}{\partial \boldsymbol{m}} \cdot [\dot{\boldsymbol{m}} f(\boldsymbol{m}, t)] \\ &= D_{\mathrm{r}}(a)\frac{\partial}{\partial \boldsymbol{m}} \cdot \left[\frac{\partial}{\partial \boldsymbol{m}}\bar{f}(\boldsymbol{n}, t) + \frac{1}{kT}\bar{f}(\boldsymbol{n}, t)\frac{\partial}{\partial \boldsymbol{m}} V_{\boldsymbol{m}}(f(\boldsymbol{m}, t))\right] \\ &\quad - \frac{\partial}{\partial \boldsymbol{m}} \cdot [\dot{\boldsymbol{m}}\bar{f}(\boldsymbol{n}, t)]. \end{aligned} \tag{A.9}$$

From the chain rule above,

$$\frac{\partial}{\partial \boldsymbol{m}} \cdot \frac{\partial}{\partial \boldsymbol{m}}\bar{f}(\boldsymbol{n}, t) = \frac{\partial}{\partial \boldsymbol{n}} \cdot \frac{\partial}{\partial \boldsymbol{n}}\bar{f}(\boldsymbol{n}, t), \tag{A.10}$$

$$\begin{aligned} &\frac{\partial}{\partial \boldsymbol{m}} \cdot \left(\bar{f}(\boldsymbol{n}, t)\frac{\partial}{\partial \boldsymbol{m}} V_{\boldsymbol{m}}(f(\boldsymbol{m}, t))\right) \\ &= \frac{\partial}{\partial \boldsymbol{m}}\bar{f}(\boldsymbol{n}, t) \cdot \frac{\partial}{\partial \boldsymbol{m}} V_{\boldsymbol{m}}(f(\boldsymbol{m}, t)) \\ &\quad + \bar{f}(\boldsymbol{n}, t)\frac{\partial}{\partial \boldsymbol{m}} \cdot \frac{\partial}{\partial \boldsymbol{m}} V_m(f(\boldsymbol{m}, t)) \\ &= \frac{\partial}{\partial \boldsymbol{n}}\bar{f}(\boldsymbol{n}, t) \cdot \frac{\partial}{\partial \boldsymbol{n}} V_{\boldsymbol{n}}(\bar{f}(\boldsymbol{n}, t)) \\ &\quad + \bar{f}(\boldsymbol{n}, t)\frac{\partial}{\partial \boldsymbol{n}} \cdot \frac{\partial}{\partial \boldsymbol{n}} V_{\boldsymbol{n}}(\bar{f}(\boldsymbol{n}, t)), \end{aligned} \tag{A.11}$$

and

$$\frac{\partial}{\partial \boldsymbol{m}} \cdot [\dot{\boldsymbol{m}} \bar{f}(\boldsymbol{n}, t)] = \boldsymbol{U}^{\mathrm{T}} \frac{\partial}{\partial \boldsymbol{m}} \cdot [\dot{\boldsymbol{n}} \bar{f}(\boldsymbol{n}, t)]. \tag{A.12}$$

Therefore, the function $\bar{f}(\boldsymbol{n}, t)$ satisfies the Smoluchowski equation:

$$\begin{aligned}
&\frac{\mathrm{d}}{\mathrm{d}t} \bar{f}(\boldsymbol{n}, t) \\
&\quad = D_{\mathrm{r}}(a) \frac{\partial}{\partial \boldsymbol{n}} \cdot \left[ \frac{\partial}{\partial \boldsymbol{n}} \bar{f}(\boldsymbol{n}, t) + \frac{1}{kT} \bar{f}(\boldsymbol{n}, t) \frac{\partial}{\partial \boldsymbol{n}} V_{\boldsymbol{n}}(f(\boldsymbol{n}, t)) \right] \\
&\qquad - \frac{\partial}{\partial \boldsymbol{n}} \cdot [\dot{\boldsymbol{n}} \bar{f}(\boldsymbol{n}, t)] \\
&\quad = D_{\mathrm{r}}(a) \mathcal{R} \cdot \left[ \mathcal{R} \bar{f}(\boldsymbol{n}, t) + \frac{1}{kT} \bar{f}(\boldsymbol{n}, t) \mathcal{R} \bar{f}(\boldsymbol{n}, t) \right] \\
&\qquad - \mathcal{R} \cdot [\dot{\boldsymbol{n}} \times \bar{f}(\boldsymbol{n}, t)].
\end{aligned} \tag{A.13}$$

The Jeffery orbit becomes:

$$\dot{\boldsymbol{n}} = \boldsymbol{U}\dot{\boldsymbol{m}} = \boldsymbol{U}(\boldsymbol{\Omega} \cdot \boldsymbol{m} + a[\boldsymbol{D} \cdot \boldsymbol{m} - \boldsymbol{D} : \boldsymbol{mmm}]). \tag{A.14}$$

It is easy to check, for the specific $\boldsymbol{U}$ defined in (27),

$$\begin{aligned}
&\boldsymbol{U\Omega} \cdot \boldsymbol{m} = \boldsymbol{\Omega} \cdot \boldsymbol{n} = (p_2 - p_3) \bar{\boldsymbol{\Omega}} \cdot \boldsymbol{n}, \\
&\boldsymbol{UD} \cdot \boldsymbol{m} = \sqrt{4p_1^2 + (p_2 + p_3)^2}\, \bar{\boldsymbol{D}} \cdot \boldsymbol{n}, \\
&\boldsymbol{UD} : \boldsymbol{mmm} = \sqrt{4p_1^2 + (p_2 + p_3)^2}\, \bar{\boldsymbol{D}} : \boldsymbol{nnn},
\end{aligned} \tag{A.15}$$

where $\bar{\boldsymbol{\Omega}}$, $\bar{\boldsymbol{D}}_{\mathrm{shear}}$ are defined in (14). Therefore, the Jeffery orbit can be written as:

$$\dot{\boldsymbol{n}} = Pe(\bar{\boldsymbol{\Omega}} \cdot \boldsymbol{n} + \bar{a}[\bar{\boldsymbol{D}} \cdot \boldsymbol{n} - \bar{\boldsymbol{D}} : \boldsymbol{nnn}]), \tag{A.16}$$

with $Pe$ and $\bar{a}$ defined in (26) and (18). This is exactly the Jeffery orbit obtained from the simple shear flow (20).

## References


[1] G.B. Jeffery, The motion of ellipsoidal particles immersed in a viscous fluid, Proc. R. Soc. London, Ser. A 102 (1922) 161–179.

[2] G.I. Taylor, The formation of emulsions in definable fields of flow, Proc. R. Soc. London, Ser. A. 146 (1934) 501.

[3] G. Astarita, G. Marrucci, Principles of Non-Newtonian Fluid Mechanics, McGraw-Hill, London, 1974.

[4] J. Feng, C.V. Chaubal, L.G. Leal, Closure approximations for the Doi theory: which to use in simulating complex flows of liquid-crystalline polymers? J. Rheol. 42 (5) (1998) 1095–1119.

[5] M. Doi, S.F. Edwards, The Theory of Polymer Dynamics, Oxford University Press, Clarendon, London, 1986.

[6] R.G. Larson, The Structure and Rheology of Complex Fluids, Oxford University Press, Clarendon, London, 1999.

[7] G.G Fuller, L.G. Leal, Flow birefringence of concentrated polymer solutions in two-dimensional flows, J. Polym. Sci. Polym. Phys. Ed. 19 (1981) 557–587.

[8] K.S. Yim, C.F. Brooks, G.G. Fuller, Non-Newtonian rheology of liquid-crystalline polymer monolayers, Langmuir 16 (2000) 4325–4332.

[9] M.G. Forest, Q. Wang, Monodomain response of finite-aspect-ratio macromolecules in shear and related linear flows, Rheol. Acta 42 (2003) 26–42.

[10] M.G. Forest, R. Zhou, Q. Wang, Symmetries of the Doi kinetic theory for nematic polymers of arbitrary aspect ratio: at rest and in linear flows, Physical Review E 66 (3) (2002) 031712.

[11] F.P. Bretherton, The motion of rigid particles in a shear flow at low Reynolds number, J. Fluid Mech. 14 (1962) 284–304.

[12] E.J. Hinch, L.G. Leal, Time-dependent shear flows of a suspension of particles with weak Brownian rotations, J. Fluid Mech. 57 (4) (1973) 753–767.

[13] H. Brenner, D.A. Edwards, Macrotransport Processes. Butterworth–Heinemann, 1993.

[14] N. Phan-Thien, R.I. Tanner, A new constitutive equation derived from network theory, J. Non-Newton. Fluid Mech. 2 (1977) 353–365.

[15] M.W. Johnson, D. Segalman, A model for viscoelastic fluid behavior which allows non-affine deformation, J. Non-Newton. Fluid Mech. 2 (1977) 255–270.

[16] V. Faraoni, M. Grosso, S. Crescitelli, P.L. Maffettone, The rigid-rod model for nematic polymers: an analysis of the shear flow problem, J. Rheol. 43 (1999) 829–843.

[17] C.V. Chaubal, L.G. Leal, G.H. Fredrickson, A comparison of closure approximations for the Doi theory of LCPs, J. Rheol. 39 (1995) 73–103.

[18] J. Remmelgas, L.G. Leal, Computational studies of the FENE-CR model in a two-roll mill, J. Non-Newton. Fluid Mech. 89 (2000) 231–249.

[19] P.L. Maffettone, M. Grosso, M.C. Friedenberg, G.G. Fuller, Extensional flow of a two-dimensional polymer liquid crystal, Macromolecules 29 (1996) 8473–8478.

[20] T. Maruyama, G.G. Fuller, M. Grosso, P.L. Maffettone, The dynamics of two-dimensional polymer nematics, J. Non-Newton. Fluid Mech. 76 (1998) 233–247.

[21] A.S. Lodge, Elastic Liquids, Academic Press, London, 1964.

[22] F. Pignon, A. Magnin, J.M. Piau, The orientation dynamics of rigid rod suspensions under extensional flow, J. Rheol. 47 (2) (2003) 371–388.

[23] T. Tsuji, A.D. Rey, Effect of long range order on sheared liquid-crystalline polymers. Part 1: Compatibility between tumbling behavior and fixed anchoring, J. Non-Newton. Fluid Mech. 73 (1997) 127–152.

[24] M.G. Forest, R. Zhou, Q. Wang, Full-tensor alignment criteria for sheared nematic polymers, J. Rheol. 47 (1) (2003) 105–127.

[25] X.Y. Zheng, M.G. Forest, R. Zhou, Q. Wang, Likelihood and expected-time statistica of monodomain attractors in sheared discotic and rod-like nematic polymers, Rheol. Acta, in press.

[26] Q. Wang, A hydrodynamic theory for solutions of nonhomogeneous nematic liquid-crystalline polymers of different configuration, J. Chem. Phys. 116 (20) (2002) 9120.

[27] M.G. Forest, Q. Wang, R. Zhou, The weak shear kinetic phase diagram for nematic polymers, Rheol. Acta. 43 (1) (2004) 17–37.

[28] M.G. Forest, Q. Wang, R. Zhou, The flow-phase diagram of Doi–Hess theory for sheared nematic polymers. Part II: Finite shear rates, Rheol. Acta., in press.